

Ageing of Diesel Aerosols

Design and Implementation of a
Teflon Simulation Chamber

Magnus Lindskog

Erik Nordin

Master Thesis

Engineering Physics



Ergonomics and Aerosol Technology
Department of Design Sciences
Lund University

ISRN LUTMDN/TMAT-5123-SE
EAT 2009

Abstract

Aerosol research is important since airborne particles have effect on both health and climate. There are many aerosol related topics that needs more research; one of them is secondary aerosol formation. This thesis work is a part of a larger research project on secondary aerosol formation from anthropogenic combustion sources. The objective of this thesis work was to implement a Teflon measurement chamber for diesel exhaust studies and to perform initial measurements in the preexisting steel chamber. Experiments where diesel exhausts from a Peugeot 405 (1994), a VW Passat (1998) and a Peugeot 307 (2004) were exposed to ozone were conducted. The experiments were monitored by SMPS (Scanning Mobility Particle Sizer) that measured the size distribution and AMS (Aerosol Mass Spectrometer) that measured the chemical composition of the particles. The results showed that no nucleated particles were formed when diesel exhausts were exposed to ozone in the steel chamber. However condensation of volatile organic compounds (VOC) on diesel agglomerate particles was present, indicating the importance of secondary aerosol formation processes after combustion aerosols are emitted to the atmosphere. The design, implementation and evaluation of a Teflon simulation chamber and measurement setup where exhausts can be exposed for ozone and UV-light was a part of this work. The functionality of the Teflon chamber was also tested through different experiments. The results showed that the chamber needs more cleaning before it could be used in future experiments and that the particle loss rate in the chamber is acceptable.

Keywords: Diesel exhaust, Simulation chambers, secondary aerosol formation, Teflon chamber, ozone, UV-light

Preface

This report is part of a larger research project called “Secondary Aerosol formation from anthropogenic combustion sources”. The aim of the research project is to get a better understanding of the formation of secondary aerosol, from the anthropogenic combustion sources: diesel engines and wood combustion. (Pagels 2007)

For practical inputs on construction of the Teflon simulation chamber a study visit to university of Copenhagen, department of Chemistry was performed.

Patrik Nilsson was involved in the SMPS calibration procedure. Axel Eriksson was the person in charge of the AMS calibration. The calibration procedures we took part in will be presented in this report as well.

Abbreviations and symbols

AMS	Aerosol Mass Spectrometer
B	Particle mechanical mobility
BFSP	Brute force single particle (measurement mode for the AMS)
C_c	Cunningham factor
CPC	Condensation Particle Counter
C_{sat}	Saturated concentration
D'	Diffusion constant
d_a	Particle aerodynamic diameter
d_m	Electrical mobility diameter
d_p	Particle equivalent diameter
d_{va}	Particle vacuum aerodynamic diameter
d_{ve}	Particle volume diameter
DMA	Differential Mobility Analyzer
e	Elementary charge
E	Electrical field strength
FEP	Fluorinated ethylene propylene
HR	High-resolution
I/I_0	Light intensity ratio
IE	Ionization efficiency
k	Boltzmann's constant
K	Coagulation coefficient
Kn	Knudsen number
L	Tube length
lpm	Liters per minute
m_p	Particle mass
MS	Mass Spectrum
m/z	Mass over charge
PM	Particulate matter
ppb	Parts per billion
ppm	Parts per million
$q_{aerosol}$	Aerosol flow rate
q_{sh}	Sheath air flow rate
RESPI	Respiratory Particle deposition Instrument
RH	Relative humidity
SMPS	Scanning Mobility Particle Sizer
SOA	Secondary organic aerosol
T	Temperature
TEOM	Tapered Element Oscillating Microbalance
ToF	Time-of-Flight
U	Voltage
ULPA	Ultra Low Penetration Air filter
V_0	Initial velocity

V_{TE}	Terminal electrostatic velocity
V_{TS}	Settling velocity
Z	Electrical mobility
η	Viscosity
λ	Mean free path
ρ_0	Standard density (1000kg/m ³)
ρ_{eff}	Effective density
σ_0	Extinction coefficient
τ	Relaxation time

Table of contents

1	Introduction.....	1
1.1	Background.....	1
1.2	Aim.....	2
1.3	Method and limitations.....	2
2	Aerosol science/theory	3
2.1	Aerosol growth and formation.....	3
2.1.1	Vapor pressure.....	3
2.1.2	Nucleation.....	3
2.1.3	Condensation.....	4
2.1.4	Coagulation.....	4
2.2	Particle size definitions and deposition mechanism.....	5
2.2.1	Cunningham factor (C_c).....	5
2.2.2	Knudsen Number (Kn).....	5
2.2.3	Diffusion.....	5
2.2.4	Sedimentation.....	6
2.2.5	Impaction.....	6
2.2.6	Electrical forces.....	6
2.2.7	Particle equivalent diameters.....	7
2.3	Atmospheric chemistry.....	8
2.3.1	Ozone/ NO_x /VOC reactions.....	8
2.3.2	Atmospheric/diesel aerosols.....	9
2.3.3	Secondary aerosol formation.....	10
3	Instrument and measurement techniques.....	11
3.1	Instrumental theory.....	11
3.1.1	SMPS (Scanning Mobility Particle Sizer).....	11
3.1.2	DMA (Differential Mobility Analyzer).....	12
3.1.3	CPC (Condensation Particle Counter).....	13
3.1.4	TEOM (Tapered Element Oscillating Microbalance).....	14
3.1.5	AMS (Aerosol Mass Spectrometer).....	15
3.1.6	Ambient Ozone Analyzer.....	18
3.1.7	NO_x Analyzer.....	18

3.2	Instrumental setup	20
3.2.1	Simulation Chambers	20
3.2.1.1	Steel chamber.....	20
3.2.1.2	Design of Teflon chamber	21
3.2.2	UV lamps	24
3.2.3	Cooling equipment	25
3.2.4	Diesel aerosol generation.....	26
4	Measurements and operation	27
4.1	Instrument calibration.....	27
4.1.1	Mass calibration - SMPS vs. TEOM.....	27
4.1.2	Number concentration calibration - SMPS vs. an external CPC	27
4.1.3	AMS calibration.....	27
4.2	Tests on cooling equipment	30
4.3	Tests on UV lamps	30
4.4	Tests on Teflon chamber	30
4.4.1	Chamber purity	30
4.4.2	Particle loss	31
4.5	Diesel measurements in steel chamber.....	31
4.5.1	Poorly functioning diesel car - Peugeot 405.....	31
4.5.2	Diesel car without particle trap - VW Passat.....	32
4.5.3	Diesel car with particle trap - Peugeot 307 SW	32
5	Results and discussion.....	33
5.1	Instrument calibration.....	33
5.1.1	Mass calibration - SMPS vs. TEOM.....	33
5.1.2	Number concentration calibration - SMPS vs. an external CPC	34
5.2	Tests on cooling equipment	35
5.3	Tests on UV lamps	35
5.4	Tests on Teflon chambers	36
5.4.1	Chamber Purity	36
5.4.2	Particle loss	38
5.5	Diesel measurements in steel chamber.....	39
5.5.1	Poorly functioning diesel car - Peugeot 405.....	40
5.5.2	Diesel car without particle trap - VW Passat.....	44

5.5.3 Diesel car with particle trap - Peugeot 307 SW	52
6 Conclusions and future work	54
References.....	55
Acknowledgements.....	58
Appendix A.....	59
Appendix B	61

1 Introduction

1.1 Background

In recent years, climate change has been a very hot topic among media, politicians and the general population. Not to mention now when media focus a lot on the melting of the polar ice and global warming. There is a lot of research on the climate effect from ambient air pollution. A not so well publicly known topic is the health effects from ambient air pollution. The European Union has a framework program called Clean Air for Europe (CAFE). They have estimated that 350 000 people die in excess every year in the EU, due to ambient particulate air pollution (Sehlstedt et al. 2007). In Sweden it is estimated that 3500 people die in excess every year due to long range anthropogenic particles (Forsberg et al. 2005).

Road traffic is responsible for a significant part of the ambient air pollution. Particulate matter (PM) from diesel exhaust has during a long time been considered as a health risk (Sehlstedt et al. 2007). Older diesel vehicles are known for their vast emissions of particles, especially soot that is visible in the exhaust plumes. Modern diesel vehicles are equipped with particle traps which have reduced the amount of soot particles. However, it does not prevent formation of secondary aerosols in the atmosphere from exhaust gases.

The research and knowledge about secondary aerosol formation are not well developed yet. This is because of the number of complicated physical and chemical processes that are involved in the formation of secondary aerosols (Hallquist et al. 2009). Because of the lack of knowledge in this area Ergonomics and Aerosol Technology (EAT) in collaboration with Nuclear Physics, Lund University, Department of Chemistry, Copenhagen University and the Department for Applied Physics and Electronics, Umeå University were granted funds from FORMAS. The overall objective of the project is to improve the knowledge of secondary aerosol formation from anthropogenic combustion sources to assist modeling of global climate change and assessments of adverse health effects.

Within the FORMAS project, secondary aerosol formation from anthropogenic combustion sources (diesel exhaust and wood burning) is studied due to exposure from ozone and UV light (Pagels 2007). To be able to expose aerosols for UV light without polluting the aerosol due to potential gas-phase emissions from the light sources some kind of enclosure is needed. The enclosure needs to be transparent for wavelengths in the UV area. In similar research (Paulsen et al. 2008; Carter et al. 2005; Presto et al. 2005) a measurement chamber manufactured in DuPont Teflon fluorocarbon film, FEP was used.

1.2 Aim

The aim of this master's thesis is:

- To design the measurement arrangement with the Teflon chamber, UV-lights and cooling equipment.
- Test and prepare the Teflon chamber for further measurements in the Formas project.
- Perform initial measurements of diesel particles that are exposed to ozone in the pre-existing steel chamber using SMPS (Scanning Mobility Particle Sizer) and AMS (Aerosol Mass Spectrometer) to characterize the particles.
- Analyze the initial measurement data and investigate the ageing of the diesel particles.

1.3 Method and limitations

A literature study was performed. It included measurement methods and research on secondary aerosol formation. We also studied the literature about similar experimental set-ups involving Teflon simulation chambers.

The ageing experiments have been performed with one type of fuel, diesel. Only ageing processes caused from reaction with ozone were studied. The experiments were monitored by SMPS (Scanning Mobility Particle Sizer) that measured the size distribution and AMS (Aerosol Mass Spectrometer) that measured the chemical composition of the particles.

2 Aerosol science/theory

The definition of an aerosol is particles, liquid or solid which are suspended in a gas. The gas is normally air. The size of the aerosol particles are about 0,002 to 100 μm . (Hinds 1999) The number concentration in clean air is about 1000 particles/ cm^3 while highly polluted air can contain as much as 1 000 000 particles/ cm^3 . (Akselsson et al. 1994)

2.1 Aerosol growth and formation

2.1.1 Vapor pressure

Consider a closed glass container, filled to half of its volume with a single liquid compound, X. An X molecule is either in liquid state or as a single vapor molecule. The partial pressure is the pressure that the vapor would exert on the glass if it was alone in the glass container. When there is a thermodynamic equilibrium between the vapor and the liquid at a given temperature, the water vapor exerts its saturation vapor pressure on the glass walls. The mass concentration in the vapor at the saturation vapor pressure can easily be obtained from the ideal gas law. It is denoted saturated vapor concentration c_{sat} .

Consider compound X in an aerosol system where the liquid phase is replaced by a number of aerosol droplets. When the total mass concentration in the system is smaller than c_{sat} , the mass will be in gas phase. If the mass concentration is higher than c_{sat} , the vapor is saturated and the difference in mass concentration will be in droplet state.

Diesel exhaust contains volatile organic compounds (VOCs) and when they are oxidized their vapor pressure will typically decrease. Since the vapor pressure is proportional to the saturated vapor concentration, c_{sat} will decrease. The result is that, a larger part of the reaction product mass concentration will be in the particle phase compared to the original compounds. There are also second order effects which affect the vapor pressure of a given compound in an aerosol particle consisting of many compounds. This includes the Kelvin effect and interactions between the different compounds in the aerosol particle, cf. Hinds, chapter 13. (Hinds 1999)

2.1.2 Nucleation

The process when particles are formed from a supersaturated vapor is called nucleation. There are four different kinds of nucleation processes:

- Homogeneous homomolecular nucleation: A particle is formed when gas molecules from the same chemical composition merge together.
- Homogeneous heteromolecular nucleation: A particle is formed when gas molecules from different kinds of chemical composition merges together.

- Heterogeneous homomolecular nucleation: A particle is formed when gas molecules with the same chemical composition accumulates on particles with different chemical composition.
 - Heterogeneous heteromolecular nucleation: A particle is formed when gas molecules with different chemical composition accumulates on particles with different chemical composition.
- (Akselsson et al. 1994)

2.1.3 Condensation

Condensation is the process when an aerosol particle (droplet or dry solid particle) grows due to gas molecules condense on it. How much the particle grows depends on particle size, saturation ratio and particle size relative to the gas mean free path. The mean free path is the average distance a gas molecule travels in the gas before it collides with another molecule. Depending on these parameters different numbers of vapor molecules will collide with the aerosol particle surface and therefore the growth will be different. (Hinds 1999; Akselsson et al. 1994)

2.1.4 Coagulation

Coagulation is when an aerosol particle collides with another aerosol particle and together forms a new one. The most common type of coagulation is thermal coagulation. It is a spontaneous reaction that occurs from the Brownian motion (cf. 2.2.3). Coagulation is a complicated process but if an assumption is made that the aerosol is monodisperse with spherical particles and only thermal movement is present, a simplified formula can be derived.

$$\frac{dN}{dt} = -KN^2 \quad (2.1)$$

$$K = 4\pi d_p D' \quad (2.2)$$

where K is the coagulation coefficient, N is the number concentration, d_p is particle diameter and D' is the diffusion constant.

The most common coagulation event is however when a small particle collides with a large particle. This is due to the often large number of small particles and to the high collision probability with large particles because of their vast surfaces. This results in a decrease in number concentration of small particles and an often negligible increase in size for the larger particles. The coagulation rate depends strongly on the particle number concentration ($\sim N^2$). For example engine exhaust that has a very high number concentration, the size distribution changes in a matter of seconds. The opposite is ambient air where this process can take several days. For aerosol concentration greater than 10^5 particles/cm³ coagulation becomes an important factor. (Hinds 1999; Akselsson et al. 1994)

2.2 Particle size definitions and deposition mechanism

2.2.1 Cunningham factor (C_c)

When the size of a particle decreases towards the mean free path of the surrounding gas molecules, the gas can no longer be considered to be a continuous medium. To compensate for this, the Cunningham factor is introduced.

$$C_c = 1 + \frac{\lambda}{d_p} \left[2,34 + 1,05e^{-0,39\frac{d_p}{\lambda}} \right] \quad (2.3)$$

where d_p is the particle equivalent diameter, λ is the mean free path. The Cunningham factor has to be taken into consideration for particles with a diameter less than 1 μm . The Cunningham factor approaches unity with increasing particle size. (Hinds 1999; Akselsson et al. 1994)

2.2.2 Knudsen Number (Kn)

The Knudsen number is defined as

$$Kn = \frac{2\lambda}{d_p} \quad (2.4)$$

where λ is the gas mean free path. The Knudsen number constitutes the flow of a gas around a particle. (Akselsson et al. 1994)

2.2.3 Diffusion

Brownian motion is the random movement of particles caused by collision between the particles and surrounding gas molecules. The net transport caused by Brownian motion is called diffusion and is described by the Stokes-Einstein's equation (formula 2.5). The transport occurs due to a concentration gradient in the chamber.

$$D' = \frac{C_c kT}{3\pi\eta d_m} = kTB \quad (2.5)$$

where C_c is the Cunningham factor, k is Boltzmann's constant, T is temperature in Kelvin, η is the viscosity of the surrounding medium, d_m is the particle mobility diameter and B is the particle mechanical mobility. Diffusion is the dominant deposition process for particles with a diameter less than 0,1 μm . Diffusion will cause small particles to deposit on walls (simulation chamber) and tubes/pipes and therefore it is of great importance in aerosol measurements. (Hinds 1999; Akselsson et al. 1994)

2.2.4 Sedimentation

Settling velocity is the velocity the particle reaches when there is equilibrium between the gravitational force and the drag force.

$$V_{TS} = \frac{\rho_0 d_a^2 g}{18\eta} \quad (2.6)$$

where ρ_0 is the standard density, d_a is the particle aerodynamic diameter, g is the gravitational constant and η is the viscosity of the surrounding medium. Sedimentation is mainly present between 0,1 and 100 μm . The settling velocity is the particles downward speed and causes them to deposit on horizontal surfaces and it is called sedimentation. This is present on floors and horizontal tubes/pipes and is therefore very important in chamber measurements. (Hinds 1999; Akselsson et al. 1994)

2.2.5 Impaction

Impaction is caused by the particle's lack of ability to follow the air stream due to its inertia. The stopping distance is used to describe how well particles can follow the air stream.

$$S = \frac{\rho_0 d_a^2 C_c V_0}{18\eta} = \tau V_0 \quad (2.7)$$

where ρ_0 is the standard density, d_a is the particle aerodynamic diameter, V_0 is the initial velocity of the particle and τ is the relaxation time. Impaction is present between 1 and 100 μm . Larger particles have longer stopping distances and therefore lesser ability to follow the air stream and will therefore deposit in narrow bends and obstacles. Since measurements often are performed on small particles, impaction is not of great importance in chamber measurements. (Hinds 1999; Akselsson et al. 1994)

2.2.6 Electrical forces

Uncharged airborne aerosol particles can become charged after colliding with ions in the surrounding air. The charge can be either positive or negative. Similarly charged particles can be neutralized after colliding with another particle with opposite charge. This will eventually lead to a Boltzmann equilibrium which means that the charge distribution is Boltzmann like.

When a charged particle is situated in an electrical field it will be affected by an electrical force. The electrical mobility (Z) can be derived when the drag- and electrical force of the particles is in equilibrium.

$$Z = \frac{V_{TE}}{E} = \frac{ne C_c}{3\pi\eta d_m} \quad (2.8)$$

where n is the number of elementary charges, e is the elementary charge, d_m is the electrical mobility diameter, E is the electrical field strength and V_{TE} is the terminal electrostatic velocity. (Hinds 1999) Deposition due to electrical forces is important when using a Teflon

chamber. The walls in a Teflon chamber build up a much larger electrical field than those in a steel chamber since Teflon is an electrically insulating material. The loss due to wall deposition can be up to 100 times larger for a single charge particle smaller than 0,5 μm than for a neutral particle of the same size. (Paulsen et al. 2005)

2.2.7 Particle equivalent diameters

Particle size is a very important feature when conduction measurements or aerosol calculations. Aerosol particles have different shapes and vary through a large span of sizes. Because of the irregular shapes, the concept of equivalent diameters has been introduced. This means that the equivalent diameter of the particle will be the diameter of a sphere with the same properties as the irregular shaped particle. Equivalent particle diameters are often defined by the measurement principle. The most frequently used equivalent diameters are:

- Aerodynamic equivalent diameter, d_a : is defined as the diameter of a sphere that has the same settling velocity as the particle. The equivalent sphere has the same density as a water droplet i.e. 1000kg/m^3 . This is the most common used equivalent diameter and many instrument (for example impactors) yields results in this diameter.
- Vacuum aerodynamic equivalent diameter d_{va} : is defined as the aerodynamic diameter in the free-molecular regime. When $\text{Kn} \gg 1$ (free-molecular regime) the air flow is no longer described as a continuum, but rather discrete collisions between the gas molecules and particles. The AMS uses this diameter. (DeCarlo et al. 2004)
- Volume equivalent diameter, d_{ve} : Is defined as the diameter of a sphere that has the same volume as the particle. This equivalent diameter is not very common due to the difficulties of measuring the volume of an irregular particle.
- Electrical mobility equivalent diameter, d_m : Is defined from the electrical mobility (formula 2.8). This is the particles size that is measured by the DMA.

To be able to compare AMS mass size distributions with SMPS volume distributions, the effective density rather than the conventional density has to be used. This is because of the different equivalent diameters that are measured by the two instruments. The effective density is identical to the bulk density for spherical particles but lower than the bulk density for non spherical particles. The formula for the effective density is

$$\rho_{eff} = \frac{d_{va}}{d_m} \rho_0 \quad (2.9)$$

where ρ_0 is the standard density, d_{va} is the particle vacuum aerodynamic diameter and d_m is the particle mobility diameter. Note that the relation between d_a and d_m scales with the square root of ρ_{eff} in the continuum regime. (DeCarlo et al. 2004)

The effective density can be used to calculate the mass of an agglomerated particle (formula 2.10).

$$m_p = \frac{\pi}{6} \rho_{eff} d_m^3 \quad (2.10)$$

2.3 Atmospheric chemistry

2.3.1 Ozone/NO_x/VOC reactions

The high temperature in combustion engines results in a reaction between N₂ and O₂ from the ambient air. This reaction forms NO_x (collective term for nitrogen oxides that originates from combustion), depending on the amount of oxygen in the engine, the ratio of NO and NO₂ varies. Ozone and UV-light is two important components in reactions with NO_x. NO reacts with ozone and forms NO₂ (formula 2.11), this implies that the level of tropospheric ozone is low in regions with high NO emissions (urban regions).



During daytime the ambient NO₂ reacts with UV-light and forms NO and O (formula 2.12).



If free oxygen atoms are present in the air, NO can also be formed without UV-light (formula 2.13).



With the oxygen molecule from formula 2.11 and oxygen atom from formula 2.12 it is also possible to form new Ozone (formula 2.14).



(Jacob 1999)

Ozone is very reactive with alkenes due to the double bonds. Alkenes such as ethene and butene are present in diesel exhaust. The reaction yields OH radicals. (Seinfeld et al. 2006) This is present during night time but during day time when UV-light is present, OH radicals are formed from formula 2.15 and 2.16.



(Jacob 1999)

The OH radicals react with most volatile organic compounds (VOCs). The OH initiated reaction schemes are mainly oxidation reactions, typically oxygen atoms are added to the VOC, which most often results in lower vapor pressures of the reaction products. As the vapor pressure decreases the compounds are more likely to exit the gaseous state and condense on pre-existing particles. When these gas to particle conversion processes occur in the atmosphere they are typically denoted secondary aerosol formation.

2.3.2 Atmospheric/diesel aerosols

There are many sources to atmospheric aerosols, both anthropogenic (road wear, combustion particles and photochemical processes) and natural (sea salt, soil dust and volcanic dust) (Hinds 1999).

Figure 2.1 shows an illustration of a diesel particle. Diesel PM consist of soot with a diameter of 15-40 nm, these particles form agglomerates with a size of about 60-100 nm. (Burtscher 2005) There is also metallic ash from the engine imbedded in the soot and condensed organic compounds. The diesel PM also consists of small nucleated particles that are formed when the warm engine exhaust passes through the colder exhaust system, before it leaves the exhaust pipe. (Maricq 2007) In this paper this is referred to as primary particles.

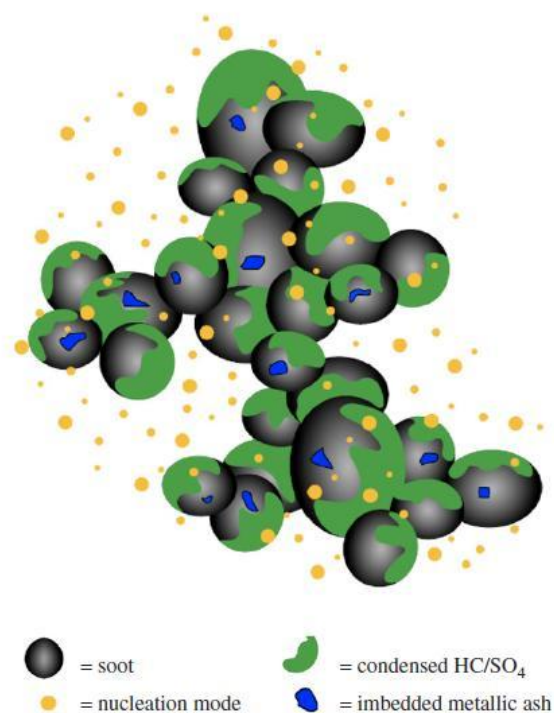


Figure 2.1: Illustration of a diesel particulate matter (Maricq 2007).

Since the diesel PM consist of agglomerates it is very difficult to define the size of the agglomerates with measurement instruments. Consider two particles with the same volume equivalent diameter, one spherical and one agglomerate. The agglomerate will have a larger mobility diameter, as the drag force is higher. Note that this implies that the effective density of the agglomerate is smaller than for the sphere to keep the mass/volume constant, cf. formula 2.10. (Burtscher 2005)

2.3.3 Secondary aerosol formation

Secondary aerosols are formed in the atmosphere, they origin from gas phase and are formed through different nucleation processes (section 2.1.2). Electromagnetic radiation, for example UV light, can induce secondary aerosol formation, cf. formula 2.15 and 2.16 (Akselsson 1994). It is uncertain which precursors secondary aerosols origin from and also how the processes work. The Science article *Rethinking Organic Aerosols: Semivolatile Emissions and Photochemical Aging* by Robinson et al., 2007 discusses a theory that a large group of volatile organic compounds and other low-volatility gas-phase species contributes to secondary aerosol formation. To examine their theory they exposed diesel exhaust to UV light. The experiment took place in a Teflon exposure chamber under atmospheric like conditions. The results of the experiment are presented in Figure 2.2. The figure shows that the amount of mass increases instantly upon UV exposure. The increase in secondary organic aerosol (SOA) formation is almost linear. They used different models to calculate the expected increase in aerosol mass (red in Figure 2.2), i.e. the formation from previous known factors. The result of the experiment shows that a larger group of compounds than previously thought is involved in SOA-formation, and that the mass increase upon UV exposure is considerably larger than previously thought. For further reading on secondary aerosol formation, cf. Hallquist et al. 2009.

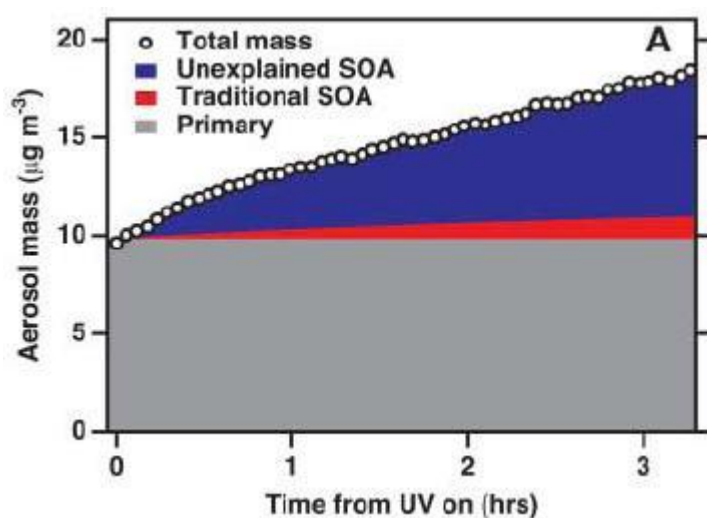


Figure 2.2: Aerosol mass as a function of exposure for UV-light (Robinson et al. 2007).

3 Instrument and measurement techniques

3.1 Instrumental theory

3.1.1 SMPS (Scanning Mobility Particle Sizer)

A SMPS is a measurement system (Figure 3.1) that consists of several components. The purpose of the system is to divide a polydisperse aerosol into several monodisperse aerosols and then be able to count the number of particles of each size. This makes it possible for the SMPS to give size distributions for the analyzed aerosol. The most important components of the SMPS are; the bipolar charger, DMA (Differential Mobility Analyzer) and CPC (Condensed Particle Counter). The system also consists of pumps, a high voltage supply and a computer with inversion software to process the data.

The SMPS-system is built at the department, it uses a custom built DMA (Hauke type), where the polydisperse aerosol enters the bottom of the DMA. The CPC is model 3010 (TSI Inc.).

The bipolar charger exposes the particles to bipolar ions. The ions collide with the particles, when equilibrium is reached; the aerosol particles have a bipolar charge distribution.

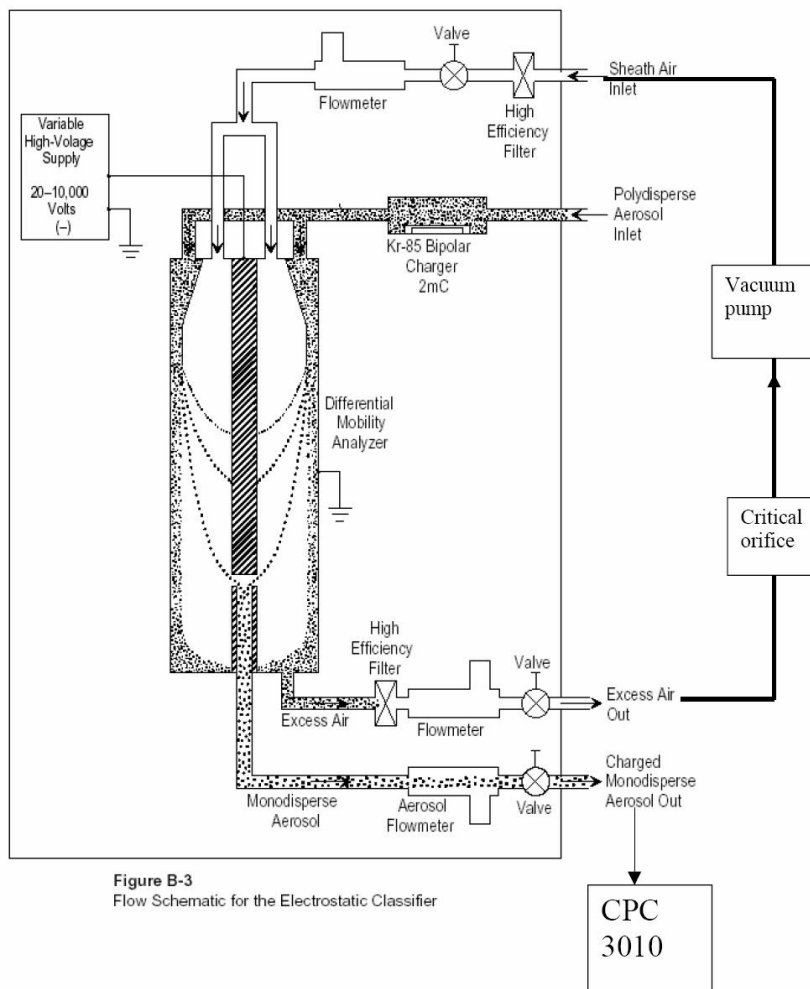


Figure 3.1: Schematic figure of the SMPS system (TSI [A]).

3.1.2 DMA (Differential Mobility Analyzer)

The DMA consists of two concentric cylinders. The inner cylinder is connected to a variable voltage supply (typically 20V to 10 000V), while the outer cylinder is grounded. This gives rise to an electrical field between the cylinders. The DMA starts on a low voltage and then continuously increases the voltage up to maximum. The succeeding scan starts from the high voltage and goes down to the minimum. Since the resulting force on the particles depends on the electrical field, the different particle sizes will be sorted out for each discrete voltage step.

Figure 3.2 shows the sheath air flow (q_{sh}) and aerosol flow ($q_{aerosol}$). We used an aerosol flow of 0,5 lpm and a sheath air flow (filtered air) of 5 lpm. The CPC uses a flow of 1 lpm and therefore an extra flow of 0,5 lpm filtered air was added after the DMA.

The electrical mobility for a particle in the DMA at a certain voltage can be calculated from instrumental parameters (formula 3.1), thus it is possible to calculate the electrical mobility equivalent diameter for a given DMA voltage. (TSI [A])

$$Z = \frac{q_{sh}}{2\pi UL} \cdot \ln\left(\frac{r_2}{r_1}\right) \quad (3.1)$$

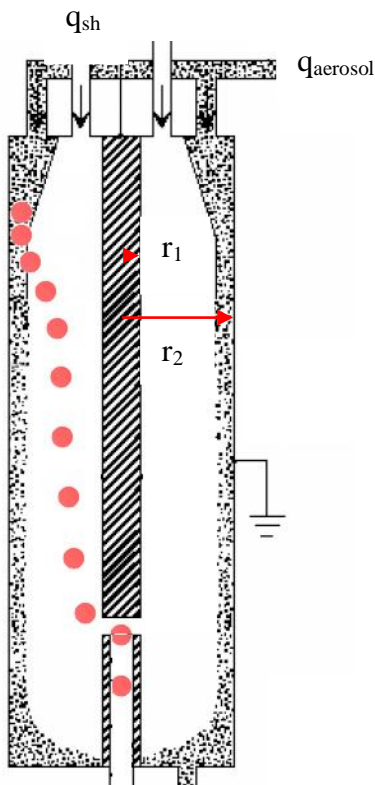


Figure 3.2: Schematic picture of the DMA (TSI [A]).

3.1.3 CPC (Condensation Particle Counter)

The function of the CPC in a SMPS system is to count the particles that the DMA have sorted out. When the aerosol enters the CPC alcohol (n-butanol) is evaporating into the heated aerosol flow. The aerosol flow is then passing through a cooled saturation block which causes the alcohol to condense on the aerosol particle. This increases their size, so they can be detected by a light scattering technique. The CPC has a cut-off diameter at 10 nm (Figure 3.4), which means that it is not possible to condensate butanol on smaller particles, due to the Kelvin effect, cf. Hinds 1999, chapter 13.2.

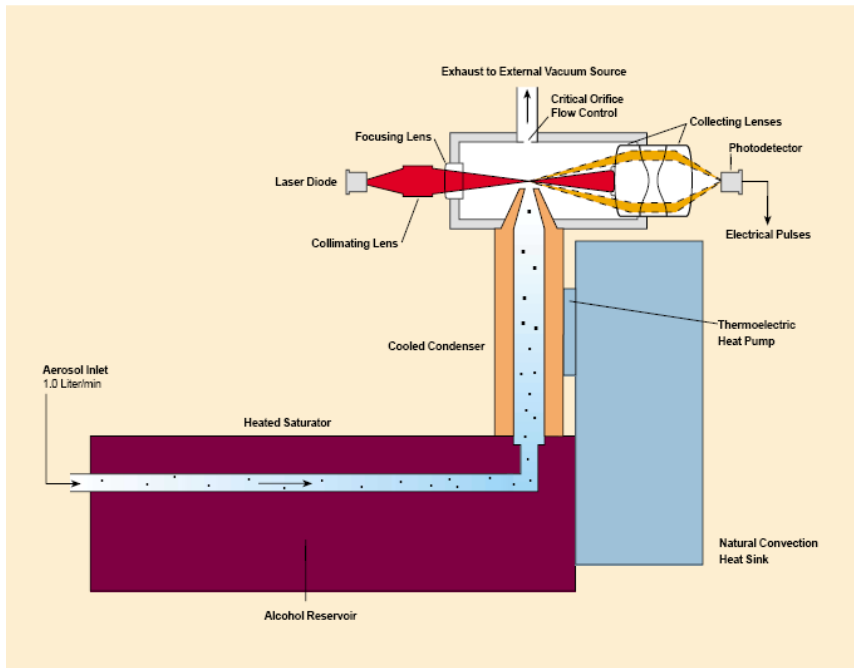


Figure 3.3: Schematic figure of the CPC model 3010 (TSI Inc.) (TSI [B]).

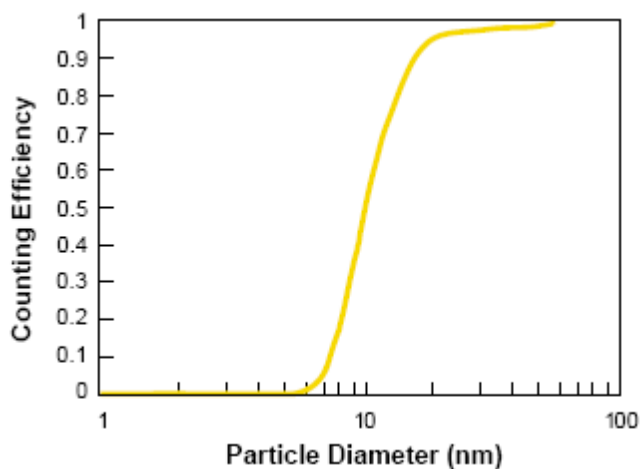


Figure 3.4: Cut-Off diameter of CPC model 3010 (TSI Inc.) (TSI [B]).

3.1.4 TEOM (Tapered Element Oscillating Microbalance)

The TEOM is a real-time instrument to measure the particle mass concentration. It consists of a tapered element made of glass with a filter on the top. The element oscillates with its eigenfrequency and when mass is collected on the filter the weight of the element changes and so does the frequency. By measuring the difference in the oscillation frequency of the element the mass concentration can be determined. To avoid that condensed water on the particles affects the result, the sampled air is heated to 30 °C to remove the water. There was also a nafion drier connected before the TEOM. The TEOM that was used is series 1 400a (Rupprecht & Patashnick). (Thermo Electronics)

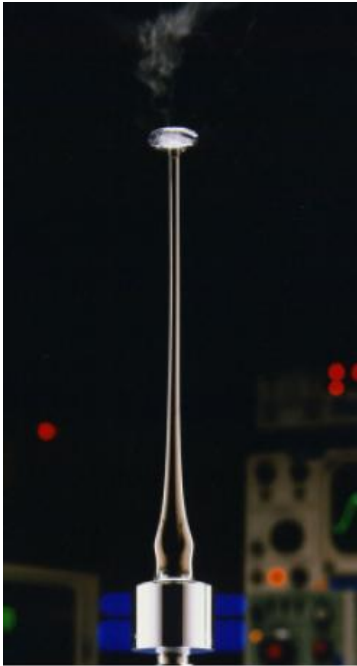


Figure 3.5: TEOM (Thermo Electronics).

3.1.5 AMS (Aerosol Mass Spectrometer)

The Aerosol Mass Spectrometer (AMS) in the Lund Aerosol Laboratory is of the type High-Resolution, Time-of-Flight, Aerosol Mass Spectrometer (HR-ToF-AMS) (Aerodyne Research Inc.).

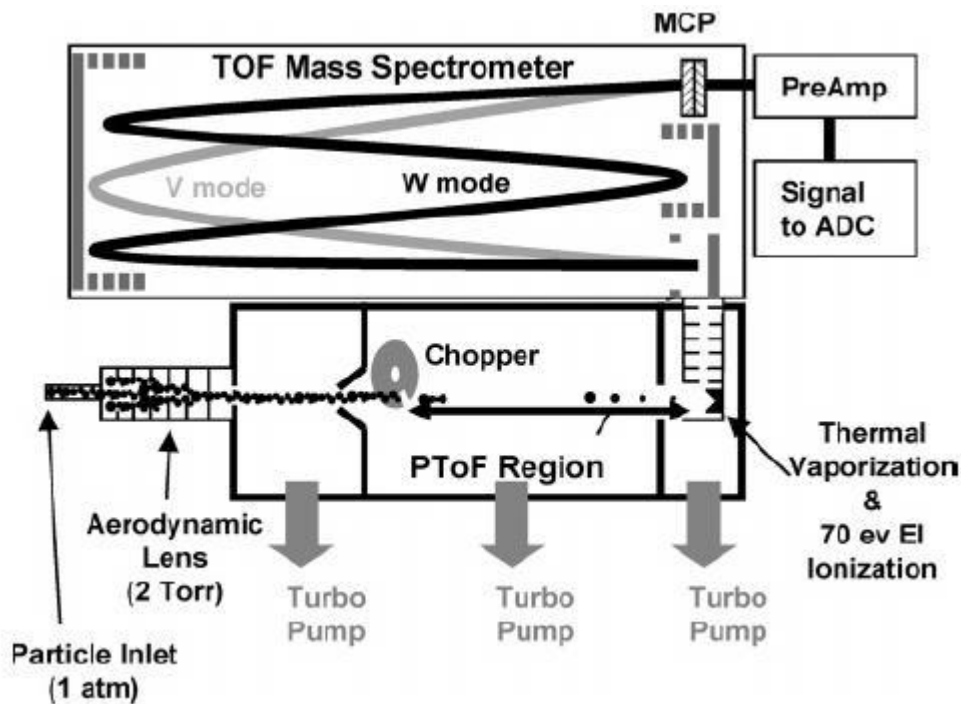


Figure 3.6: Schematic figure of the HR-ToF-AMS (DeCarlo et al. 2006).

A schematic figure of the AMS is seen in Figure 3.6. It consists of five elemental parts, aerodynamic lens inlet, chopper for size selection, vaporizer, electron emitting filament (ionizer) and the Time-of-Flight Mass Spectrometer (ToF-MS). The AMS operates under high vacuum, measurement on our instrument shows a pressure of about $1,7 \cdot 10^{-10}$ bar. The aerosols enter the inlet and pass through the aerodynamic lens. The aerodynamic lens focuses the particles to a narrow beam (Figure 3.7).

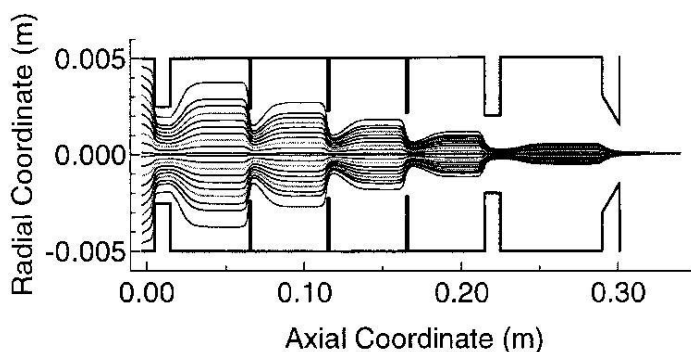


Figure 3.7: The aerodynamic lens that focuses the air beam (Jayne et al. 2000).

On the particles way to the vaporizer they pass through a chopper, which is a rotation disk with a small slit. The chopper has three modes, open, closed or chopping. In the last mode the disk spins and a small amount of particles gets through. This is used when the instrument is in PToF mode (Particle Time of Flight). The vaporizer has a temperature of about 600°C and when the particles hit the surface the non-refractory elements evaporate. After the evaporation stage the molecules become ionized to positive ions due to the bombardment of electrons from the electron emitting filament. The positive ions then enter the ToF-MS. The ToF-MS measures the time of flight for the specific ion.

The AMS can operate in two different modes, PToF and MS-mode (Mass spectrum mode). It is possible to run them one by one, but the most common way is to alternate them every 20 seconds (the period used during our experiments) during a measurement. PToF measures the vacuum aerodynamic diameter of the particles, by recording the time of flight from when the particle passes the chopper until it is detected in the ToF-MS. The time range for the particle to move from the chopper to the inlet of the ToF-MS is milliseconds, while the time range in the ToF-MS is microseconds. Within MS-mode, the time of flight in the ToF-MS of the positive ions is measured. Pending the weight, the ion is affected differently of the electrical field in the ToF-MS i.e. the time of flight is different. Using calibration software the recorded time in the ToF-MS is translated to a specific mass (m/z). The specific mass is the mass divided by charge (the ions are predominantly singly charged). For example the positive oxygen ion O^+ has m/z 16. The mass fragments are used to identify different molecules/species (Table 3.1). The ion/mass-fragments in bold type are most frequently used in the identification (Canagaratna et al. 2007).

Table 3.1: The most common mass fragments in the AMS spectra (Canagaratna et al. 2007).

Group	Molecule/Species	Ion Fragments	Mass Fragments
Water	H_2O	$\xrightarrow{e^-}$ H_2O^+ , HO^+ , O^+	18 , 17, 16
Ammonium	NH_3	$\xrightarrow{e^-}$ NH_3^+ , NH_2^+ , NH^+	17, 16 , 15
Nitrate	NO_3	$\xrightarrow{e^-}$ HNO_3^+ , NO_2^+ , NO^+	63, 46 , 30
Sulfate	H_2SO_4	$\xrightarrow{e^-}$ $H_2SO_4^+$, HSO_3^+ , SO_3^+ SO_2^+ , SO^+	98, 81, 80 64 , 48
Organic (Oxygenated)	$C_nH_mO_y$	$\xrightarrow{e^-}$ H_2O^+ , CO^+ , CO_2^+ $H_3C_2O^+$, HCO_2^+ , $C_nH_m^+$	18, 28, 44 43 , 45, ...
Organic (hydrocarbon)	C_nH_m	$\xrightarrow{e^-}$ $C_nH_m^+$	27,29, 41 , 43 ,55,57,69,71...

Since the AMS in Lund is of the type HR-ToF it is possible to use two different modes, V or W mode (Figure 3.6). The difference between those modes is the length that the ions travel. A longer distance means longer time of flight, which increases the resolution but decreases the sensitivity. A typical time of flight in V mode is about 30 μs and in W mode 50 μs (DeCarlo et al. 2006). Figure 3.8 shows the maximum resolution of the different versions of the AMS. In the V and W mode, it is possible to distinguish the different mass fragments in each peak. As seen in Figure 3.8 peak m/z 43 actually consists of five different ion fragments.

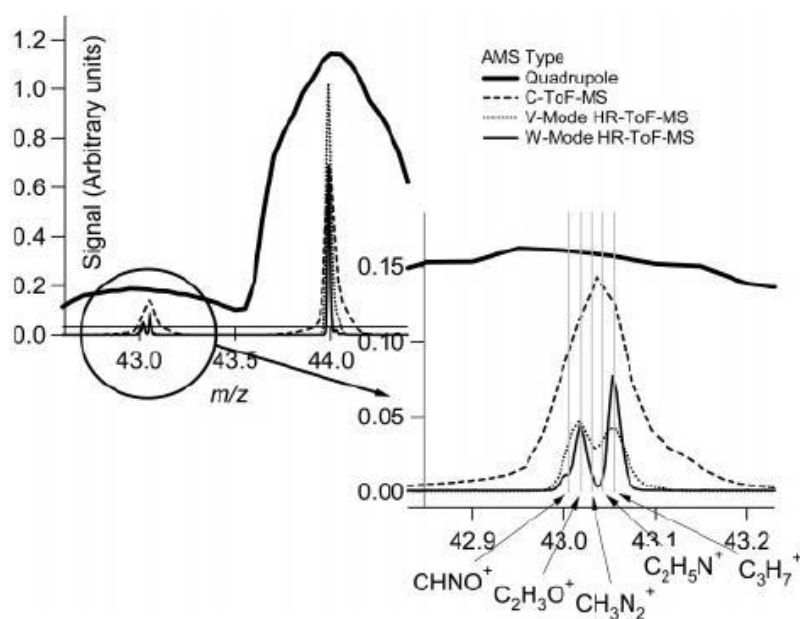


Figure 3.8: The maximum resolutions of the different versions of AMS (DeCarlo et al. 2006).

There are three different softwares to analyze the collected AMS data. Within SQUIRREL a first order analysis (unity resolution) is conducted. The software uses the PToF data to plot a mass size distribution of the different species shown in Table 3.1. From the MS-mode data it is possible to receive plots including the following:

- Mass versus time of the different species.
- Mass spectrum of the different m/z .
- The relationship between two different m/z .

Second order analyzes is performed with the software PIKA. With PIKA (high resolution) it is possible to receive the different fragments from each m/z peak. The last software is APES (plug-in to PIKA) which performs elementary analysis which yields the amount of C, H, N, O and S in every peak.

The AMS always uses the same colors to represent the different species in the diagrams from the software. Green – Organics, Blue – NO_3 , Red – SO_4 , Orange – NH_4 and Magenta – Chloride.

3.1.6 Ambient Ozone Analyzer

The ozone instrument uses the principle of the ozone's absorption of UV-light. Lambert-Beers law (formula 3.2) yields the ozone concentration.

$$\frac{I}{I_0} = e^{-\sigma_0 L} \quad (3.2)$$

where σ_0 is the extinction coefficient, L is the path length of the light beam and I/I_0 is the light intensity ratio (Hinds 1999). The low pressure Hg discharge lamp emits light at 253,7 nm. The absorption of UV-light by the ozone molecule is very high at this wavelength. To make sure that the instrument only measures the absorption from ozone molecules and no other molecules the instrument has two chambers. One that is filled with the sample air and one where ozone has been removed. The difference in absorption between the two chambers yields the ozone concentration. (NILU 2001) The instrument that was used for determining the ozone level was model 49 (Thermo electron instruments).

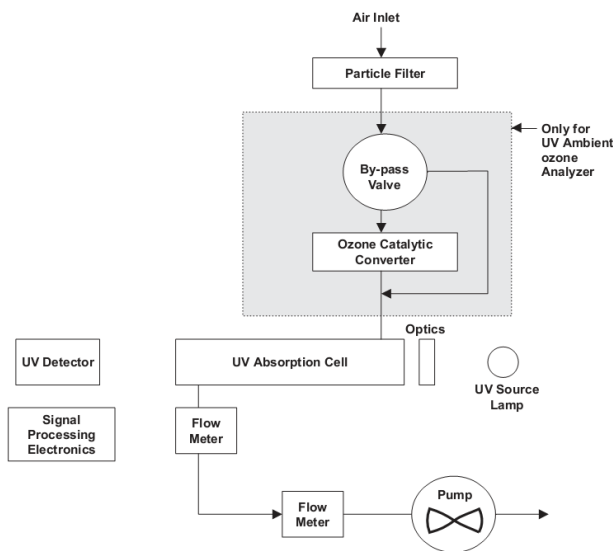


Figure 3.9: Schematic figure of Ozone analyzer (NILU 2001).

3.1.7 NO_x Analyzer

The instrument directly measures the concentration of NO and NO_x by a chemiluminescence process and can therefore also indirectly determine the NO₂ concentration. The inlet air is divided into two reaction chambers, one for NO_x and one for NO (Figure 3.10). Before the air enters the NO_x reaction chamber it passes a molybdenum converter, where the NO₂ fraction of NO_x is converted to NO (formula 3.3) at 325 °C.



Just before entering the reaction chamber the inlet air is mixed with ozone to convert NO into NO₂, about 20% of the generated NO₂ becomes excited (formula 3.4).



The excited NO_2^* then returns to its ground state, emitting energy in form of electromagnetic radiation.



The electromagnetic radiation is measured and is also proportional to the NO concentration in the sample. The NO_x analyzer used is CLD 700 AL (Eco Physics). (ECO Physics [A] 1996)

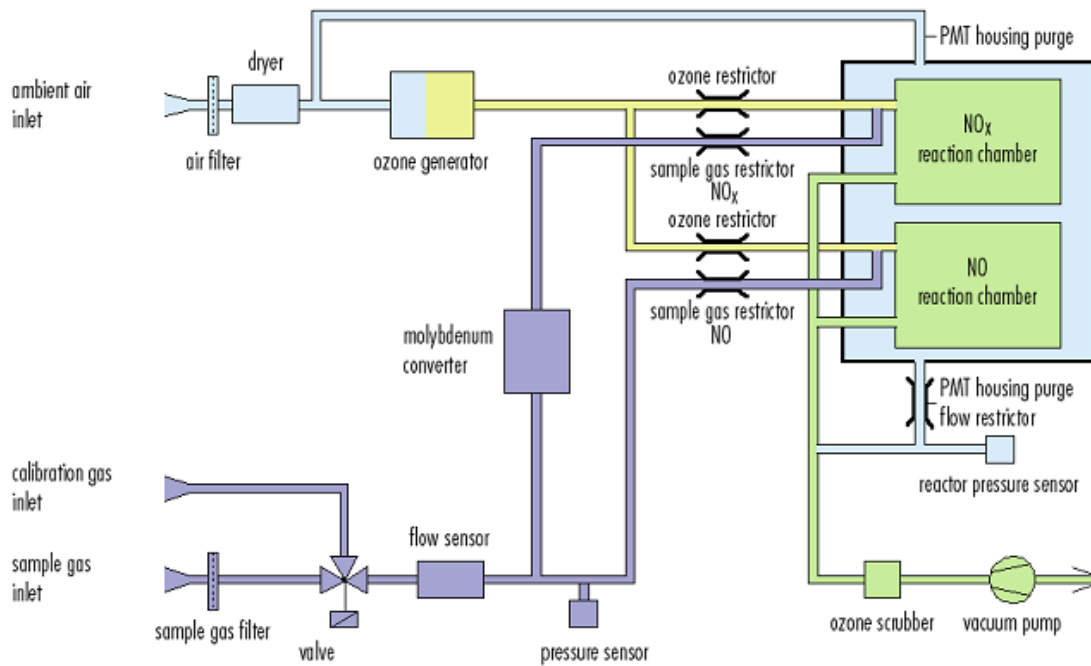


Figure 3.10: Schematic figure of NO_x analyzer (ECO Physics [B]).

3.2 Instrumental setup

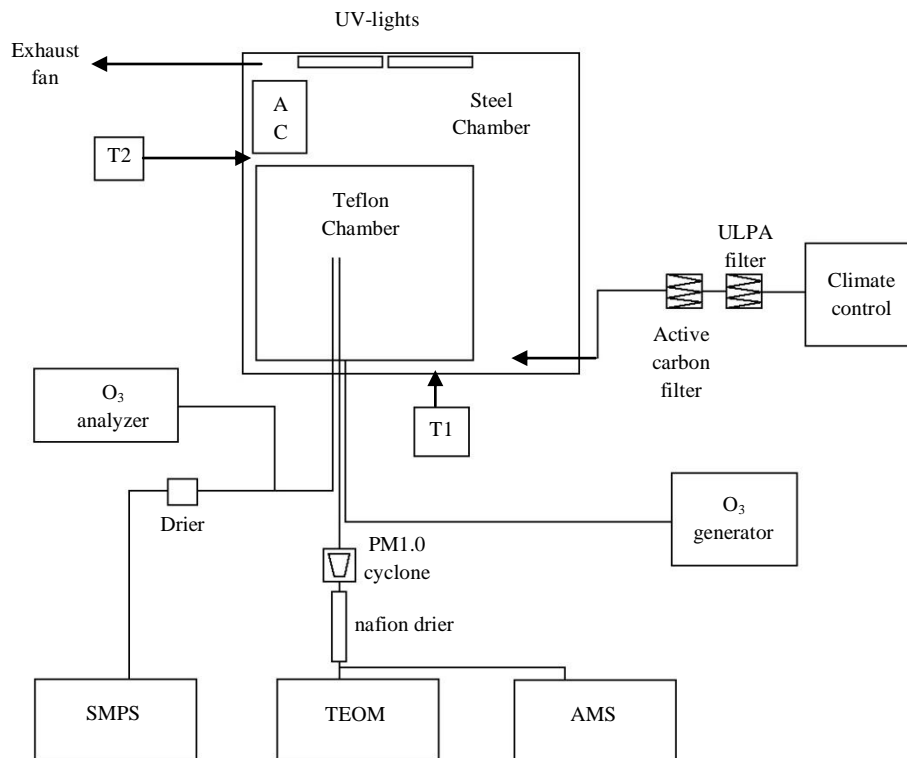


Figure 3.11: Schematic figure of the measurement setup when the Teflon chamber was in use. In ageing measurements of diesel exhaust a similar set-up excluding the Teflon chamber and UV-lights, was used. T₁ and T₂ are thermometer positions in the steel chamber.

3.2.1 Simulation Chambers

Aerosol experiments performed in laboratory often uses some kind of chambers. This is because it is easy to control temperature, RH etc., the experimental air won't be polluted and if the experiment air is toxic the chamber protects the researcher. Two different kinds were used in this Master thesis (steel and Teflon chamber).

3.2.1.1 Steel chamber

The steel simulation chamber is a 2,99 x 2,99 x 2,39 = 21,4 m² big "room" in the aerosol laboratory at the division of Ergonomics and Aerosol technology (Figure 3.12). It is a closed chamber where the operator can control the temperature, RH, pressure, supply and exhaust air flows. The inlet air passes through a set of different filters (active carbon and ULPA, Ultra Low Penetration Air filter) so it is particle free and free of pollutant gases such as VOCs and oxidants when it enters the chamber. For more information about the steel chamber cf. Isaxon 2008.



Figure 3.12: The steel chamber in the Aerosol laboratory in Lund.

3.2.1.2 Design of Teflon chamber

The Teflon chamber is manufactured by Welch Fluorocarbon Inc. (Dover New Hampshire USA). The Chamber is 1,52 m x 1,83 m x 2,13 m = 5,95 m³ (5 x 7 x 6 feet)(Figure 3.13). Three ¼” kynar fittings (Jaco 15-4) and one ¾” kynar fitting (Jaco 15-12) are placed on three of the four vertical sides (Figure 3.17) (Jaco 2007). The Jaco 15-4 fittings are predrilled so that the inner diameter will be ¼”, so a ¼” measurement tube can be inserted through the fitting.

The specifications of the Teflon chamber were designed as part of this work. The size of the Teflon chamber and placement of kynar fittings were designed to fit both the steel chamber in Lund and the exposure chamber at University of Umeå, where ageing of wood combustion aerosols is planned.

The Teflon is of the type 5 mil DuPont Teflon fluorocarbon film, FEP. We chose the 5 mil (125 µm) film because of the higher durability. FEP is used because of its high UV transmission. Paulsen et al. 2008 studied the UV transmission from FEP and DuPont Tedlar (TST and TUT) and found that FEP had the highest transmission (<90 %).

Inputs about the relationship between size and the amount of UV-light came from present chambers described in literature (Paulsen et al. 2008; Presto et al. 2005; Carter et al. 2005). Presto et al. 2005 uses a 10 m³ Teflon bag and 75 General Electric model 10526 black lights (40 W each, 3000 W in total). Paulsen et al. 2008 use a 27 m³ 5 mil FEP Teflon chamber with four xenon arc lamps (4 kW each, 16 kW in total). Carter et al. 2005 use two parallel 90 m³ 2 mil FEP Teflon chambers with one 200 kW Argon arc lamp and 80 Sylvania 350BL black lights (115 W each, 9200 W in total).

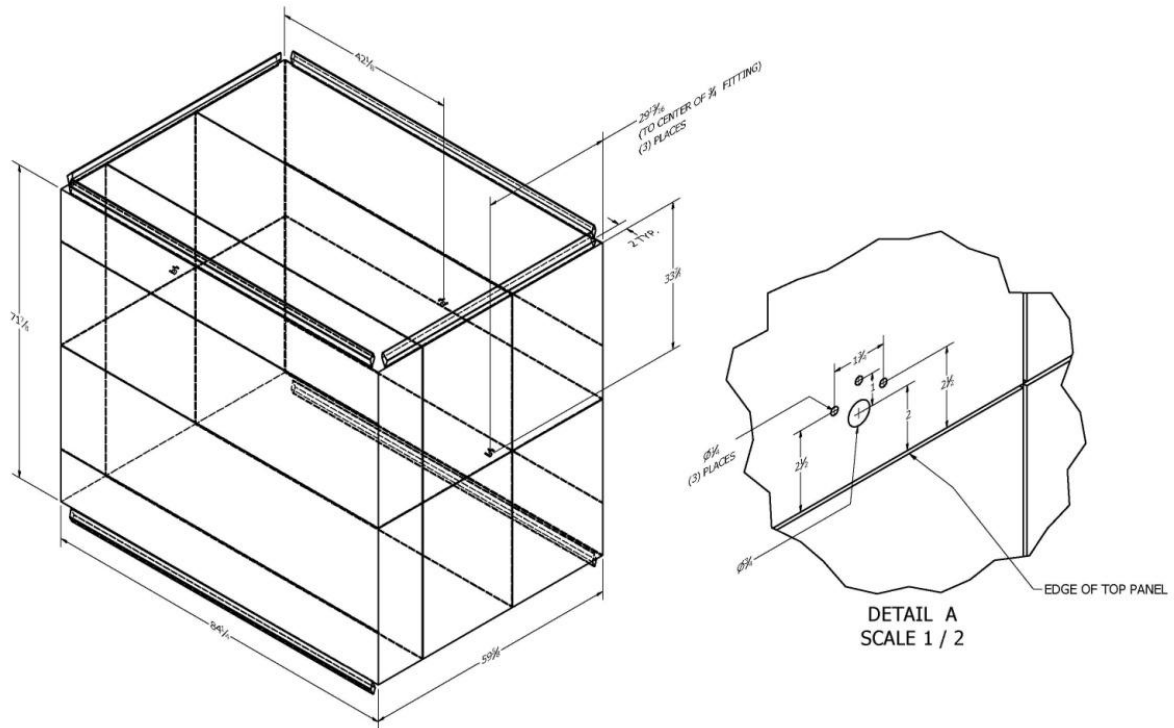


Figure 3.13: Cad sketch of the Teflon chamber (left) and a close up of the fittings (right).

The Teflon simulation chamber is suspended in an aluminum frame mounted inside the steel chamber. The frame is built from 30 mm aluminum profiles from Rexroth, Bosch Group.



Figure 3.14: The Teflon chamber and air inlet/outlet connections.



Figure 3.15: Measurement setup with Teflon chamber, AC and UV armatures.

The inlet and outlet air to the Teflon chamber is connected to the same ventilation system as the steel chamber. It is only possible to use the ventilation to one chamber at the same time.



Figure 3.16: The suspending system of the Teflon chamber.



Figure 3.17: Kynar fittings on the Teflon chamber.

3.2.2 UV lamps

Ultraviolet (UV) fluorescent tubes were chosen as light source. The model is CLEO Performance 100W –R SLV 1768x 38 mm (Philips) with a built in reflector, 200° of the tubes are covered with reflecting material which means that the UV-light is emitted in a 160° angle. This lamp was chosen because of the low UVB/UVA ratio (0,8 %). The UV lights should have an intensity peak at about 350 nm. (Philips 2009) This was chosen because among others Carter et al. 2005 used this kind of UV light. It would also be possible to use arc-lamps but they would have emitted much more heat and demanded a much more complex cooling solution. The spectrum from Carter et al. 2005 and from the CLEO Performance is very similar (Figure 3.18 and Figure 3.19)

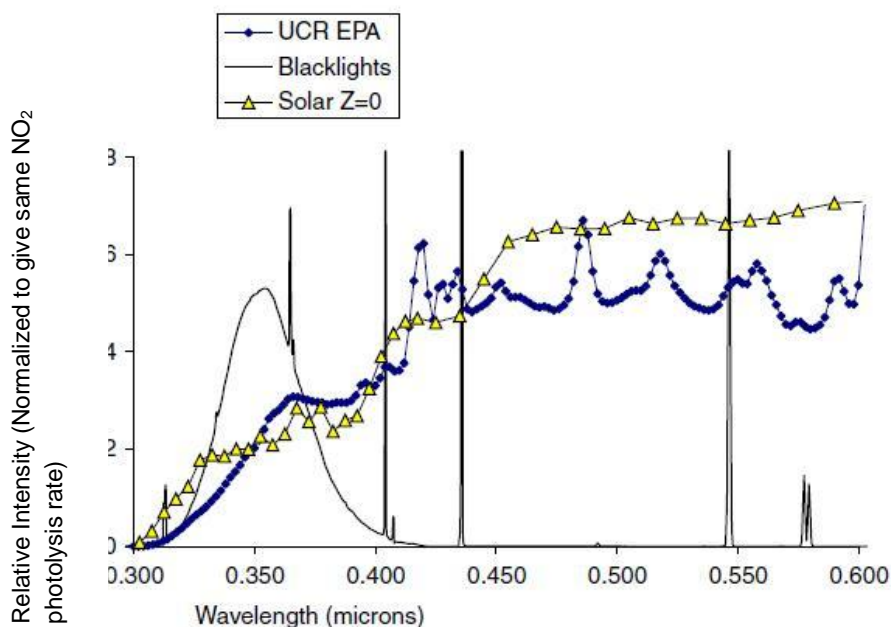


Figure 3.18: Spectrum of lights used in Carter et al. 2005.

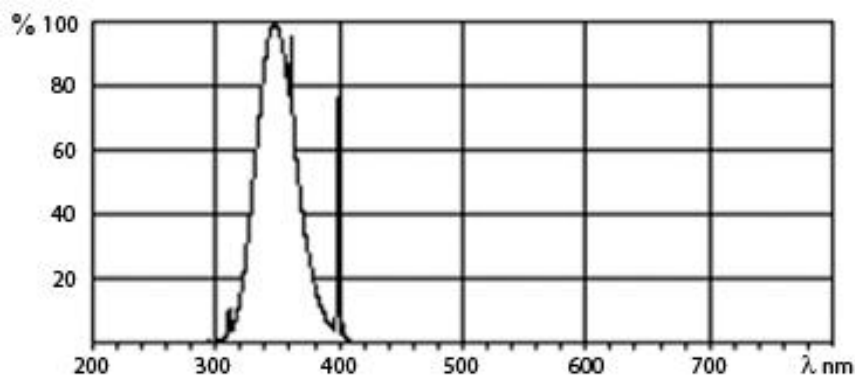


Figure 3.19: Spectrum of Philips UV-lamps (Philips 2009).

As initial armature, two used tanning beds were purchased. One with six lamps and one with ten lamps.

3.2.3 Cooling equipment

During experiments it is important to keep a constant temperature in the measurement chamber. Fluctuations in the temperature will change the vapor pressure which will change the dynamics between the particle and gas phase of a large fraction of the secondary aerosol components. An increase in temperature can cause many compounds in an aerosol particle that would normally be in particulate state to transform into gaseous state. This will affect the measurements because we mainly study aerosols in the particle phase. (Pathak et al. 2008)

Since UV-lamps emit a high amount of heat the need for cooling in the chamber is necessary to keep a stable temperature. The cooling equipment used was a domestic air conditioner of the model Linda KY-26/A (Polarpumpen). The maximum cooling effect is 2,6 kW.



Figure 3.20: The AC Linda KY-26/A (Polarpumpen).

3.2.4 Diesel aerosol generation

The experimental aerosol has been exhaust from different personal diesel cars. The construction of the generation system was performed by a fellow Master Thesis worker, Patrik Nilsson. About 10 % of the exhaust from the diesel car at idling load was injected to the dilution system by a connection to the cars tailpipe. In the dilution system the exhaust is mixed with clean air until desired dilution is reached. For further reading about the diesel generation system cf. Nilsson 2009.

4 Measurements and operation

4.1 Instrument calibration

To secure the quality of the measurements a calibration of the involved instruments are crucial. The Respi-SMPS (Respiratory Particle deposition Instrument - SMPS) were calibrated against a TEOM and a stand-alone CPC.

4.1.1 Mass calibration - SMPS vs. TEOM

The calibration aerosol was ammonium sulfate dissolved in water (2-3 % $(\text{NH}_4)_2\text{SO}_4$), which was generated through a nebulizer. The aerosol was injected into the 21,4 m³ steel chamber. The SMPS and TEOM were connected to the chamber with different tubes, from the same location, both instruments used driers, a diffusion drier for the SMPS and a nafion drier for the TEOM, the RH after drying was typically below 20%. Since the upper scan limit of the SMPS is 1000 nm a PM_{1,0}-cyclon were connected before the TEOM.

4.1.2 Number concentration calibration - SMPS vs. an external CPC

The second part of the Respi-SMPS-calibration was to compare its CPC (model 3010, TSI Inc.) to an external one (model 3022, TSI Inc.). The same calibration aerosol as in the previous experiment was generated. The calibration took part in two steps. First the external CPC was connected to the steel chamber at the same location as the SMPS. The results from the stand-alone CPC were manually collected and compared to the number concentration that the SMPS software gave. Then the CPC 3010 was disconnected from the RESPI-SMPS and the results from both CPC's were collected manually.

4.1.3 AMS calibration

The AMS ionization efficiency (IE) calibration was performed using a monodisperse 350 nm aerosol of ammonium nitrate. The initial step was to generate a polydisperse aerosol through a nebulizer. The aerosol was injected in the steel chamber. A 350 nm aerosol was selected using a DMA with constant voltage and connected to the AMS aerosol inlet.

At first we used a mode in the AMS data acquisition program called BFSP (Brute force single particle) (Figure 4.1). The BFSP mode controls the chopper so that only a small number of particles are let through. To calculate the IE the TOF-MS has to measure on a single particle and it takes about 30 minutes to collect 200 usable detections from single particles, because of the difficulties to only let one particle through the chopper. When the TOF-MS has a usable detection it saves a file with the information about ion size, mass spectrum and the electrical signal that the ion gives rise to in the TOF-MS. Since the density of ammonium nitrate and the shape factor of the particles is known it is possible to calculate its mass. With the calibration program IE Cal it is then possible to analyze the data and calculate the IE for ammonium nitrate. The IE is ions per particle (detected with the AMS) divided by molecules per particles (calculated from DMA settings). In the end this yields the relationship between

mass concentration and signal strength. It can be assumed that IE increases linearly with increasing molecule size (Aerodyne Research, Inc 2009) and therefore the IE for other molecules can be determined. It is important to have the correct IE, otherwise the mass loadings in the measurements will be incorrect.

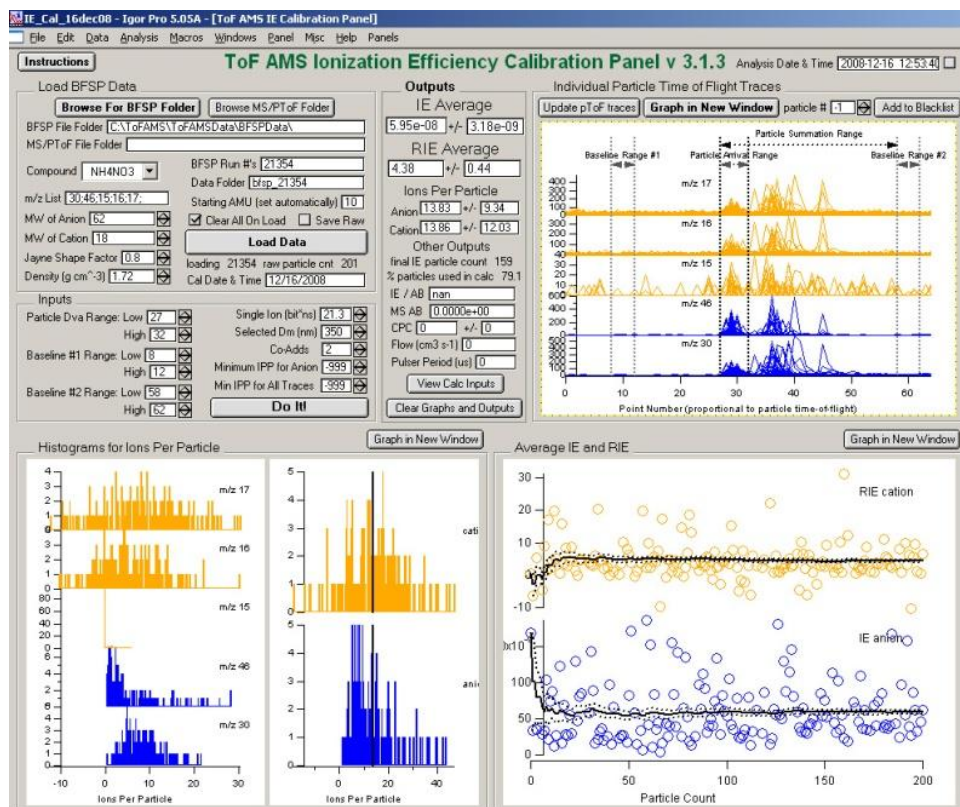


Figure 4.1: AMS IE calibration software.

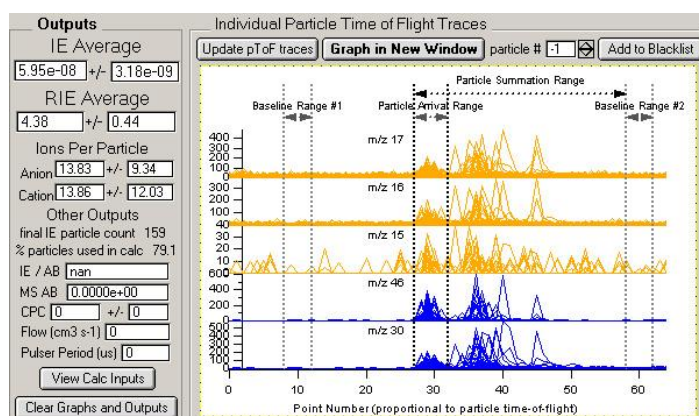


Figure 4.2: Close up AMS IE calibration software. Every particle detection gives rise to a curve. This window is used to select the single charged particles that always appear around point number 30.

Another more automatic calibration of the AMS is the m/z calibration (Figure 4.3). The purpose of the m/z calibration is to fit the measured m/z to the theoretical. This is done for ambient air molecules of higher abundance for example N_2 ($m/z = 28$) and O_2 ($m/z = 32$). Since the vaporizer consist of tungsten ($m/z = 184$), tungsten fragments will always be present. This makes it possible to make a valid calibration for high m/z .

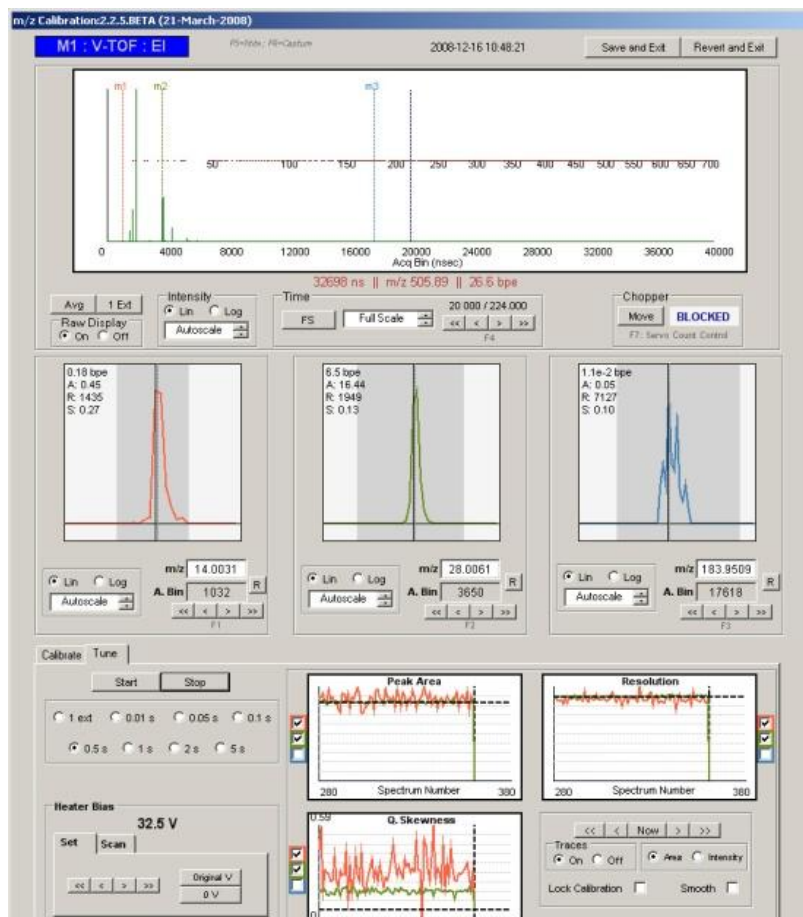


Figure 4.3: AMS m/z Calibration software.

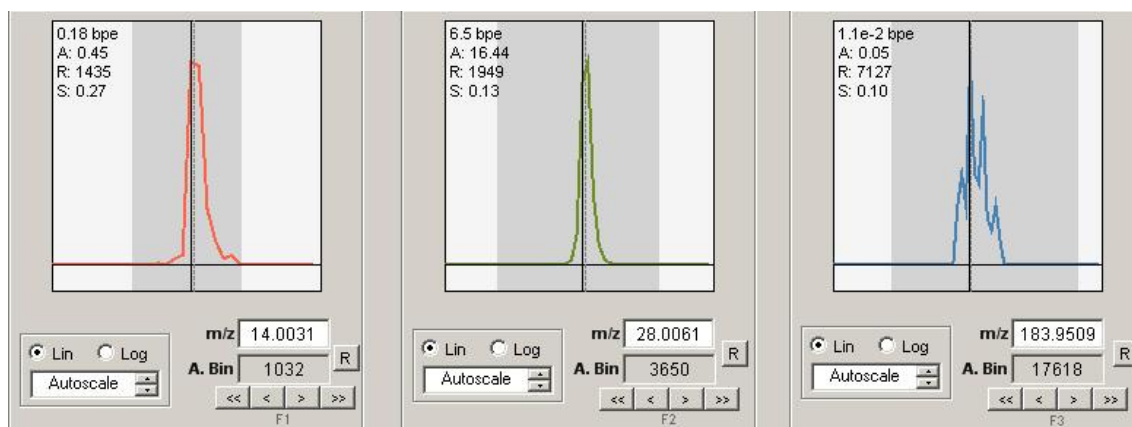


Figure 4.4: Close up AMS m/z Calibration software. This window is used to center the peak i.e. fit the measured signal to the known theoretical.

4.2 Tests on cooling equipment

To test the need for cooling we used the 16 tubes (1600 W) for 15 minutes in the chamber. The temperature rose 4,3 °C for thermometer 1 (T_1) and 5,2 °C for thermometer 2 (T_2), cf. 3.2 *Instrumental setup* for thermometer position in steel chamber (note that the Teflon chamber was not installed during this test). After installing the air conditioning system, new measurements of the temperature were conducted. The build in climate control was also used.

Lamp power: 1600 W

Climate control temperature: 15 °C

AC temperature: 15 °C

Steel chamber exhaust fan: 0

Pressure: 10 Pa under-pressure

4.3 Tests on UV lamps

We also measured the spectrum of the Philips UV-lamps to make sure that the given specification agreed with the true spectrum. The measurement took place one meter from the UV-lights. We also performed measurements from 2 meters distance and from four different angles. The reflectance of the steel chamber was also tested by aiming the UV spectrometer against the back wall (2,5 meters distance from UV lights). The UV spectrometer has a very narrow (small space angel) light inlet.

4.4 Tests on Teflon chamber

The Teflon chamber is totally new equipment in the laboratory and therefore the operation of it is totally unknown. It is also newly manufactured and it is therefore probable that it contains impurities. The particle loss rate and investigation of potential leaks is also of great importance.

4.4.1 Chamber purity

The purity of the chamber is very important since too high impurities will ruin any experiment in the chamber, therefore we investigate particle concentrations and nucleation of particles using a purity test. There are different ways to clean the chamber. The first step was to use clean air to flush out the contaminated air in the chamber. When the air was sufficiently clean (< 100 particles/cm³, < 0.1 μm³/cm³), a high rate (up to 750 ppb) of ozone was injected in the chamber. The ozone is very reactive and will react with impurities that are left in the chamber and the chamber walls itself. When ozone reacts with impurities, particles are created through nucleation. The particles can be flushed out from the chamber and the impurities vanish through the reaction. The reaction with wall impurities and evaporation of material attached to the walls can also be enhanced by exposing the chamber for high temperature. In our case we used the UV lamps to raise the temperature in the steel chamber to about 35 °C. The UV

radiation itself can also react with impurities and is therefore also a cleaning procedure. The wall impurities can be substantial and this process must be repeated several times until there is no nucleation observed when ozone is added.

To test the degree of impurities remaining, the chamber was filled with clean air. Then 200 ppb of ozone was injected. 200 ppb of ozone was used because this was the same amount that was used in the first diesel car experiments. The closed chamber was then monitored by SMPS for about 1 hour to study if there were any particle growth processes.

4.4.2 Particle loss

Since the chamber is designed to study particle formation it is important to determine the particle loss rate, i.e. how many particles that vanish through deposition mechanisms. This was conducted by injecting an ammonium sulfate aerosol into the chamber. The aerosol was generated by a nebulizer that forms particles from ammonium sulfate dissolved in water (2-3 % $(\text{NH}_4)_2\text{SO}_4$). Before the particles entered the chamber they were dried and passed through a Ni-63 bipolar charger. After the charger the particles have a Boltzmann equilibrium charge distribution. To avoid a dominating coagulation process we used a relatively small number concentration of particles (initially around 2000 cm^{-3}).

4.5 Diesel measurements in steel chamber

Measurements on diesel exhausts that were exposed for ozone were performed using three different cars, an older Peugeot 405 (1994), a VW Passat (1998) and a newer Peugeot 307 (2004). The cars were running for 10-30 minutes and then the steel chamber was ventilated until the desired concentration was reached. This was not done with the Peugeot 405 measurements where the initial concentration was used in the experiment. To aid the mixing in the steel chamber a regular domestic fan was placed inside. After the desired concentration was reached, ozone was added (200-400 ppb) to the chamber, using an ozone generator (Ozone Technology). The reason for the high ozone concentration was due to the high NO-concentration in the exhausts. A lower concentration of ozone would mainly have been consumed by the NO as the reaction rate between ozone and NO is high. After the ozone was added, continuous measurements were performed for about an hour (see Appendix B.1 for information about the experimental procedure).

4.5.1 Poorly functioning diesel car - Peugeot 405

The old Peugeot 405 was not equipped with a particle trap. Due to the bad condition (the car was deregistered) of the car it was used in the first two experiments to test the new diesel generating system. The first experiment on 4th December the car was running for 30 minutes and we used 200 ppb of ozone. The next experiment on 5th December the car was running for 10 minutes instead and we used the same ozone concentration, 200 ppb.

4.5.2 Diesel car without particle trap - VW Passat

The VW Passat was from 1998 and in much better condition. The car was used on a daily basis and therefore much better suited for the experiment. The VW Passat is also a common diesel car in Sweden. The 1998 model was not equipped with a particle trap. There were two measurements performed on the VW Passat, on the 11th of December and 18th of December. During both measurements the ozone concentration was 400 ppb and the car was running for about 25 minutes.

4.5.3 Diesel car with particle trap - Peugeot 307 SW

The last car we used was a Peugeot 307 SW equipped with a particle trap. This car was used to study how the particle trap influences the exhaust aerosol. The car was running for about 30 minutes and the ozone concentration injected was 400 ppb.

5 Results and discussion

5.1 Instrument calibration

5.1.1 Mass calibration - SMPS vs. TEOM

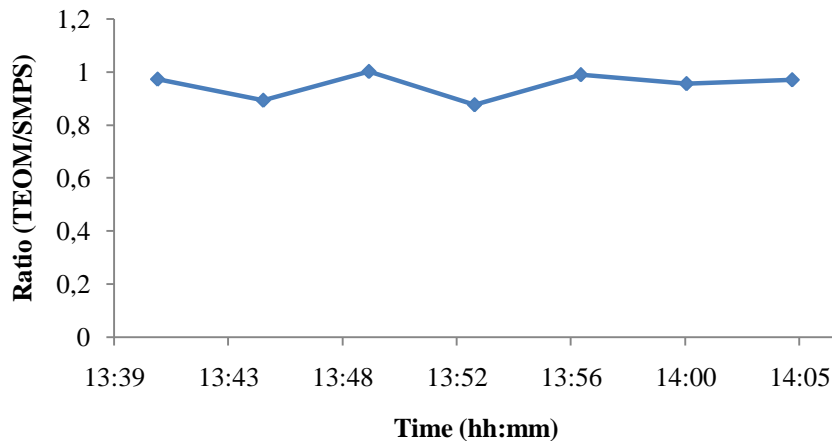


Figure 5.1: Mass concentration ratio between the TEOM and SMPS (mean value of 0,95).

Figure 5.1 shows the ratio between the TEOM mass concentration and the SMPS ditto. The ratio is very close to one, which shows good coherence between the TEOM and SMPS data. The SMPS had a scan time of 240 s (to make the measurements more exact), while the TEOM gave values every 60 s. Since the SMPS gives volume concentration and the TEOM mass concentration, the SMPS data were multiplied with $1,77 \text{ g/cm}^3$ which is the density of ammonium sulfate, spherical particles were assumed.

5.1.2 Number concentration calibration - SMPS vs. an external CPC

The results from the calibration of the SMPS vs. an external CPC are presented in Figure 5.2 and Figure 5.3. The number concentration peaks at 50-60 nm.

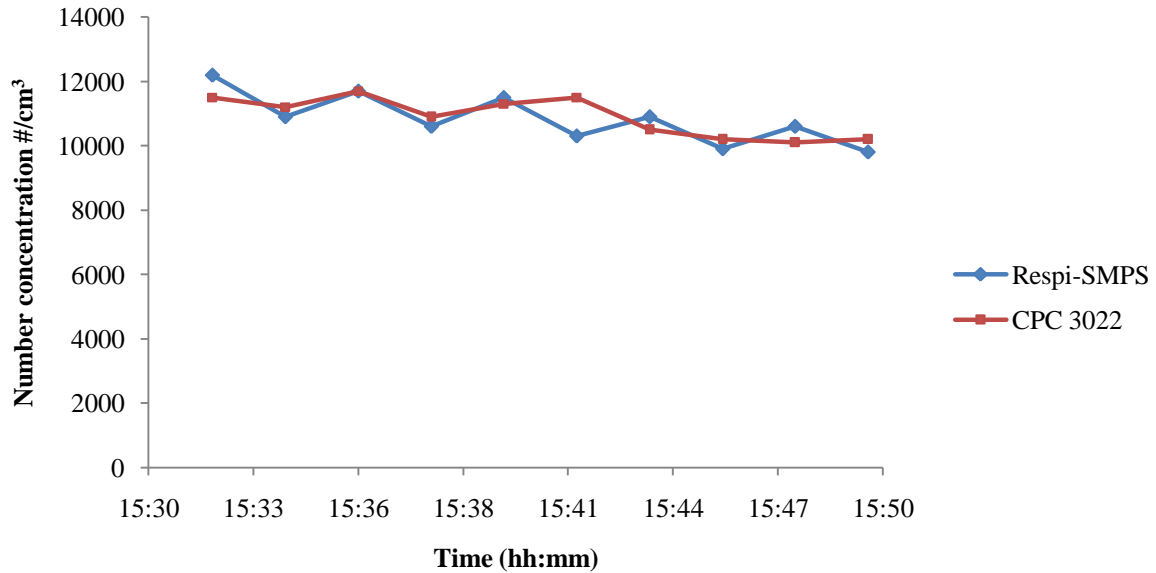


Figure 5.2: Number concentration measured by CPC 3022 and Respi-SMPS system.

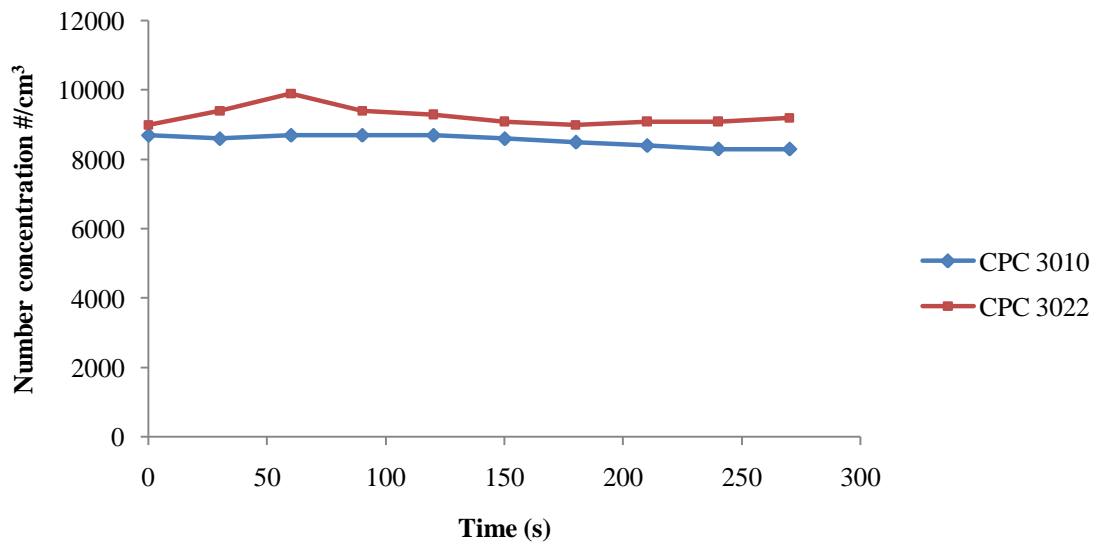


Figure 5.3: Number concentration measured by CPC 3022 and CPC 3010. The CPC 3010 was disconnected from the Respi SMPS system.

The results are very good for a calibration.

5.2 Tests on cooling equipment

The result of the test is presented in Table 5.1 and Figure 5.4. The temperature increased rapidly during the first two hours but then it was quite stable.

Table 5.1: Different temperatures after a specific time during test of the cooling equipment

Time (min)	T1	T2
0	17,2	15
30	21,6	20,8
60	24,1	22,3
90	25,1	23,5
120	25,8	23,9
150	26,3	24,6
180	26,7	24,9
210	27,1	25,7
240	27,4	25,7

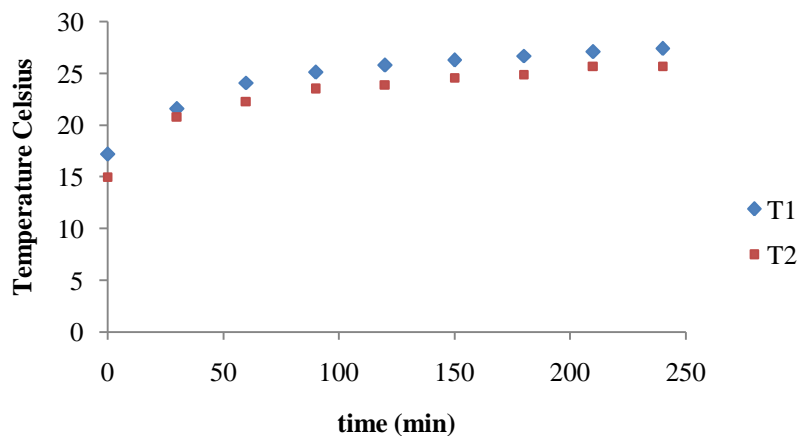


Figure 5.4: Temperature vs. time at two different locations during test of the cooling equipment.

The test of the cooling ability shows that the air condition and built in climate control provides a much more stable temperature than without any cooling equipment. If the temperature in the chamber is about 25 °C when the UV-lights start the fluctuation of the temperature could be within 3 °C which is important for the ageing experiments.

5.3 Tests on UV lamps

From the measured UV-spectra the background radiation of about 750 intensity counts has been subtracted in the spectrum. The data behind Figure 5.5 shows that the intensity peaks at 349,1 nm. The intensity spectrum was equal from every position. This is because of the built in reflectors in the UV-lights. The reflectance test showed a minimal reflectance, about 500 intensity counts on the back wall (2,5 meters from the UV-lights).

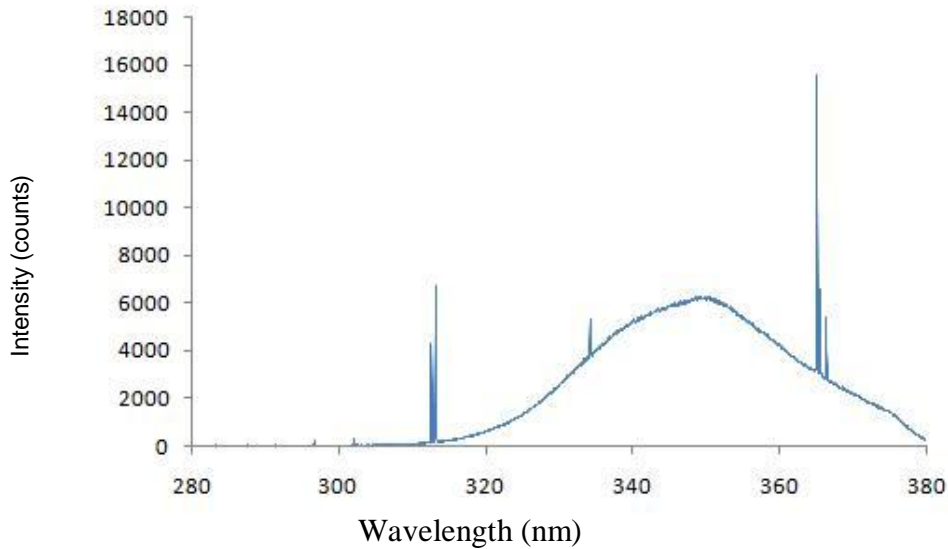


Figure 5.5: Measured UV-spectrum of CLEO Performance 100 W –R SLV (Philips) UV-lamps.

This test concludes that the light intensity should be in principle the same over the entire Teflon chamber. It also proves that the spectrum provided by Philips (Figure 3.19) agrees well with the measured spectrum. The only difference is the height of the peak around 365 nm, but since it is so narrow it has a minor effect.

5.4 Tests on Teflon chamber

5.4.1 Chamber Purity

After three days of intense cleaning of the chamber with heated air, UV light and a high amount of ozone, the chamber purity was tested. When the experiment started the number concentration was 8,6 particles/cm³ and the volume concentration was 0,01 μm³/cm³. The ozone was injected during three minutes starting at 12:42. The results of the difference in number concentration are presented in Figure 5.6 and the volume concentration in Figure 5.7. The results show that the ozone reacted very fast with impurities when it entered the chamber.

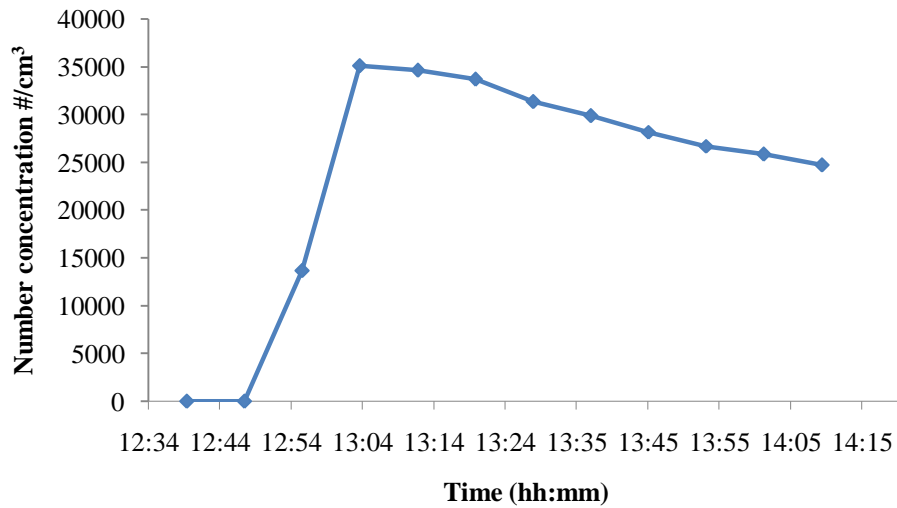


Figure 5.6: Number concentration in the Teflon chamber during purity test.

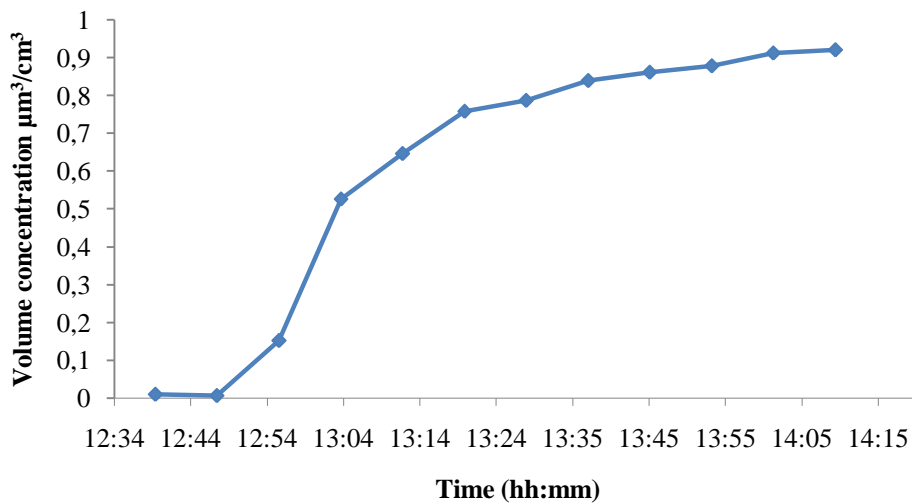


Figure 5.7: Volume concentration in the Teflon chamber during purity test.

The high amount of new formed particles implies that the chamber was not clean and therefore it needs more cleaning before any significant experiments could be performed. It may also imply that the newly installed active carbon filter or the connections downstream the filters introduce impurities. Another option that should be tested is using, pressurized air. It is expected that active carbon filters are more efficient at higher pressures.

5.4.2 Particle loss

The experiment started with an initial number concentration of about 2100 particles/cm³. During the first hour there was a rapid decrease in number concentration (Figure 5.8). Then the decrease declined and about 300 particles were lost during the next six hours. Figure 5.9 shows the normalized particle concentration for different particle sizes during the experiment.

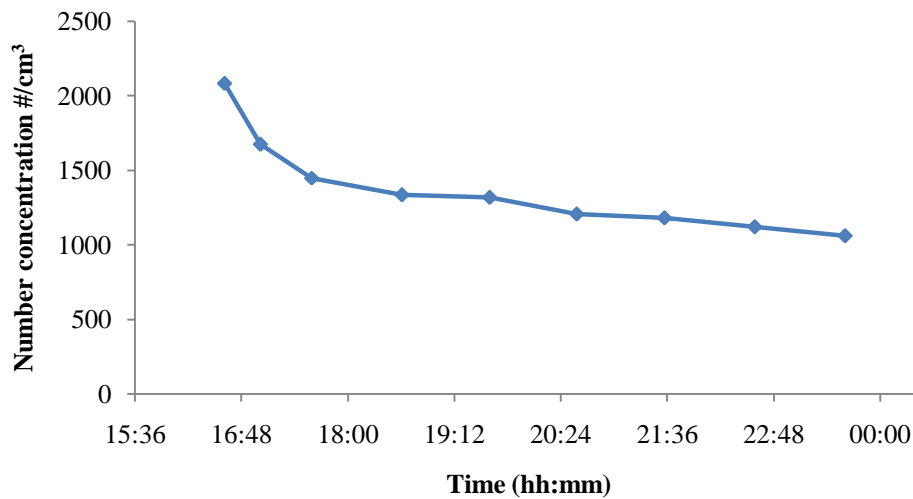


Figure 5.8: Change in number concentration during the particle loss test in the Teflon chamber.

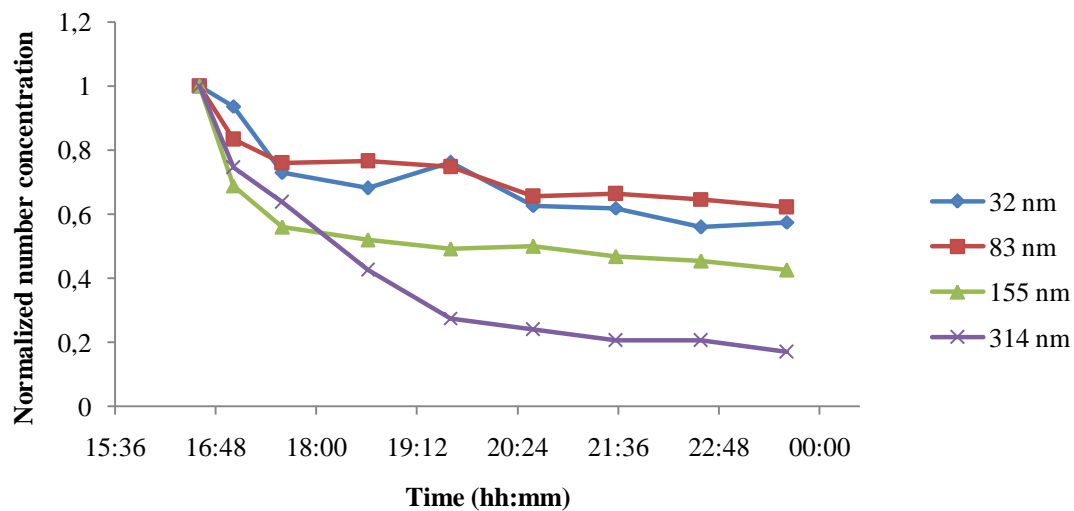


Figure 5.9: Normalized number concentration for different sizes during the particle loss test in the Teflon chamber.

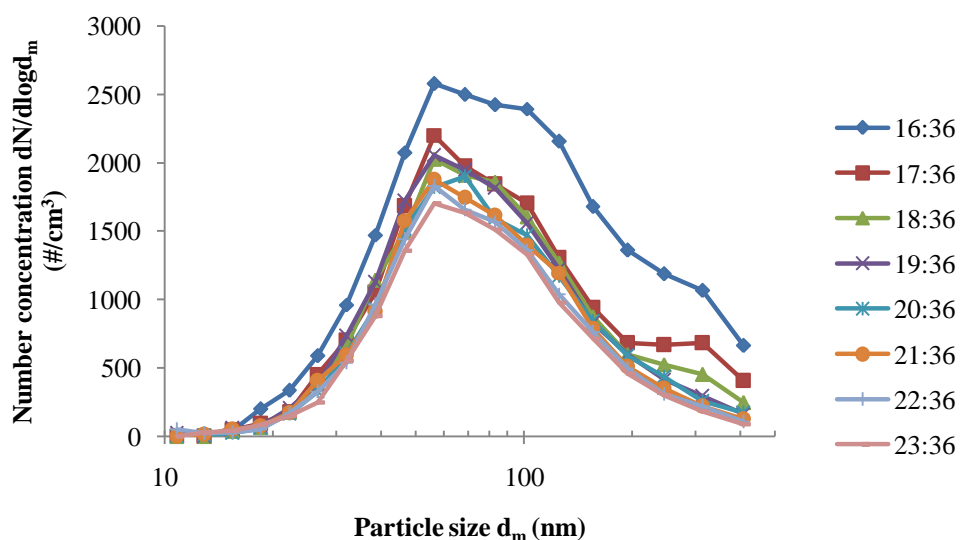


Figure 5.10: Change in number distribution during the particle loss test in the Teflon chamber.

The rapid decrease of particles in the beginning is most likely due to electrostatic forces. The Boltzmann equilibrium charge distribution contains some positively and negatively charged particles. The larger the particles are, the higher the charged fraction is. The particles that are charged will deposit rapidly on the Teflon chamber walls in the beginning. When the charged particles have deposited the decrease in particle concentration is low and likely due to diffusion and/or sedimentation. Figure 5.9 shows that the losses due to electrostatic forces (the steeper slope in the curve) take more time for the large particles (314 nm than for the smaller sizes. This is because larger particles have lower electrical mobility than the smaller particles. The loss rate due to regular deposition processes (diffusion and/or sedimentation) can be determined from the flack part of the curves in Figure 5.9. This implies that the particle loss in the chamber is acceptable, and ageing processes over up to 10 h can be studied in future experiments.

5.5 Diesel measurements in steel chamber

Table 5.2: Summary of diesel car experiments

Diesel car	Initial ozone conc. (ppb)	Initial NO conc. (ppb)	Condensation?	Nucleation?
Peugeot 405 (Exp. 1)	200	3000	NO	NO
Peugeot 405 (Exp. 2)	200	2000	NO	NO
VW Passat (Exp. 1)	400	100	YES	YES
VW Passat (Exp.2)	400	270	YES	NO
Peugeot 307 SW (Exp. 1)	400	360	N/A*	YES

* AMS out of order

5.5.1 Poorly functioning diesel car - Peugeot 405

The ozone was added during 4,5 minutes starting 15:29. Figure 5.11 and Figure 5.12 shows the result as number distribution and volume distribution. The second mode (large particle size) in Figure 5.12 is probably due to ghost particles in the DMA, likely created by a non-ideality of the geometry of this DMA, resulting in spark formation at high field-strengths. This was discovered after the first VW Passat measurements and to avoid this in the following experiments the upper limit of the scan range was set to 600 nm. Figure 5.11 shows a decrease in number concentration over time and also a slight increase in particle size.

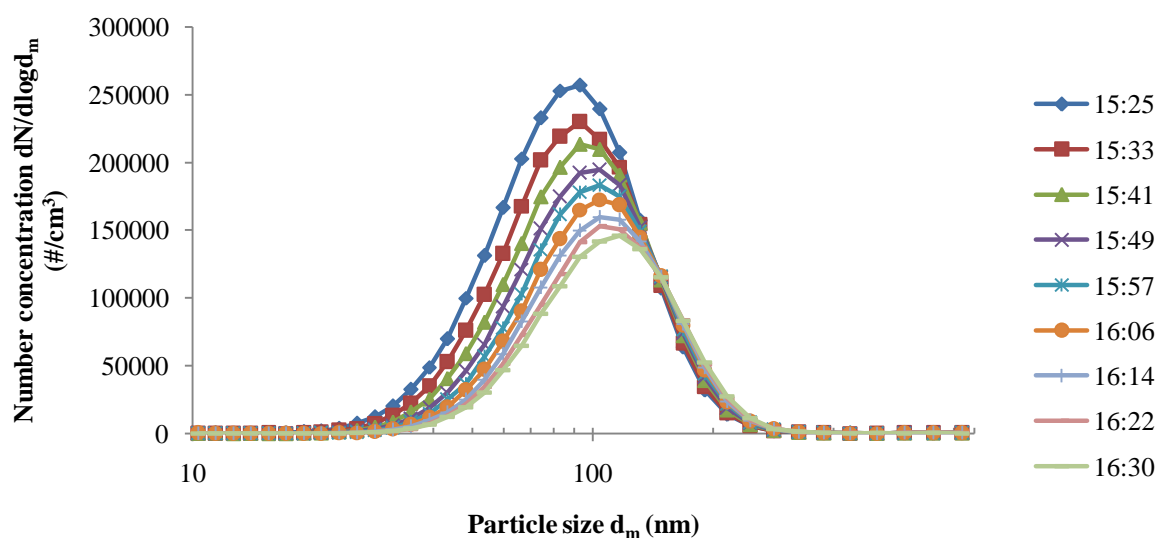


Figure 5.11: Number distribution of the first experiment with the Peugeot 405.

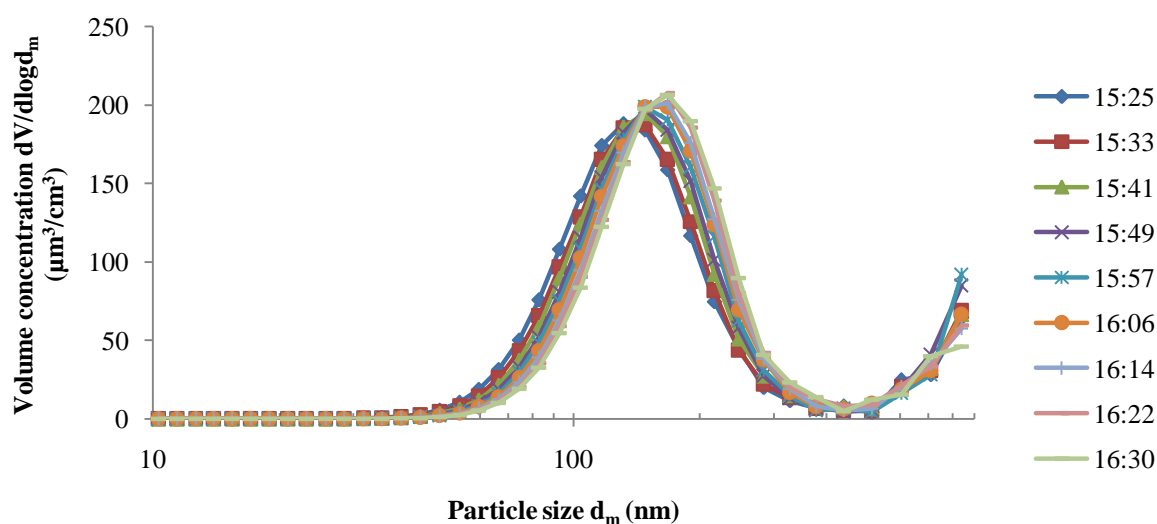


Figure 5.12: Volume distribution of the first experiment with the Peugeot 405.

Figure 5.13 shows the mass vs. time from the AMS. With the AMS no difference was noticed, just a slight decrease in organic mass over time.

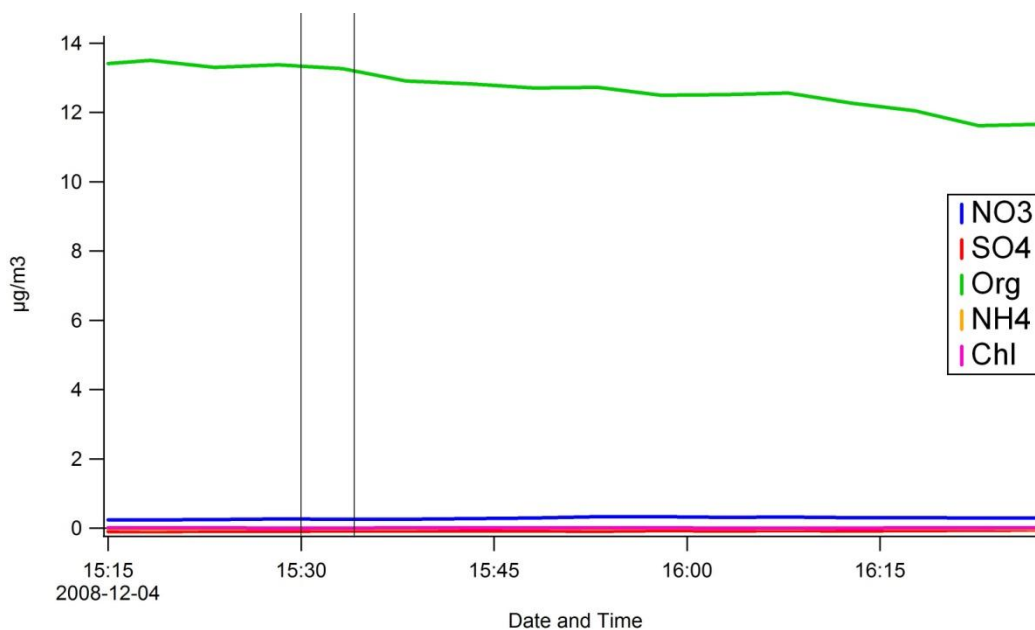


Figure 5.13: AMS, mass concentration vs. time of the first experiment with the Peugeot 405. The vertical lines indicate the time for ozone injection

Due to the high particle concentration, coagulation will have a strong effect on the number distribution. The first experiment shows no nucleation and no effect when the ozone was added. The losses in the steel chamber are much lower, as it is made of an electrically conducting material.

The second experiment with the Peugeot 405 was a repetition of the first experiment. The results in Figure 5.14 and Figure 5.15 agree well with the results in Figure 5.11 and Figure 5.12. The volume concentration in the second experiment is lower than in the first one. This is because the car was running for much longer time in the first experiment. In those first two experiments the measurement started when the number concentration was around 300 000 particles/cm³.

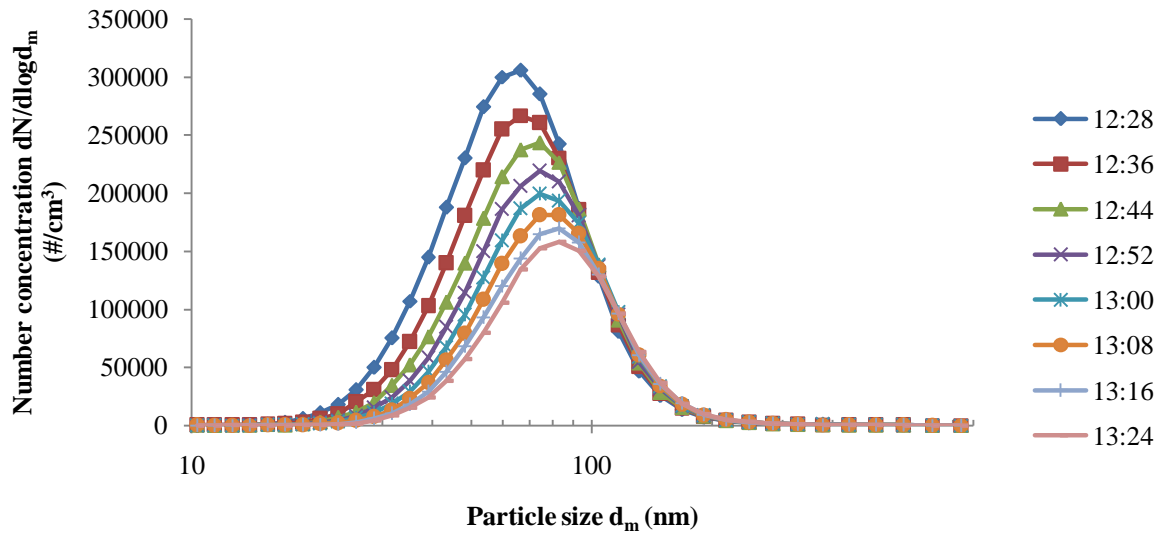


Figure 5.14: Number distribution of the second experiment with the Peugeot 405.

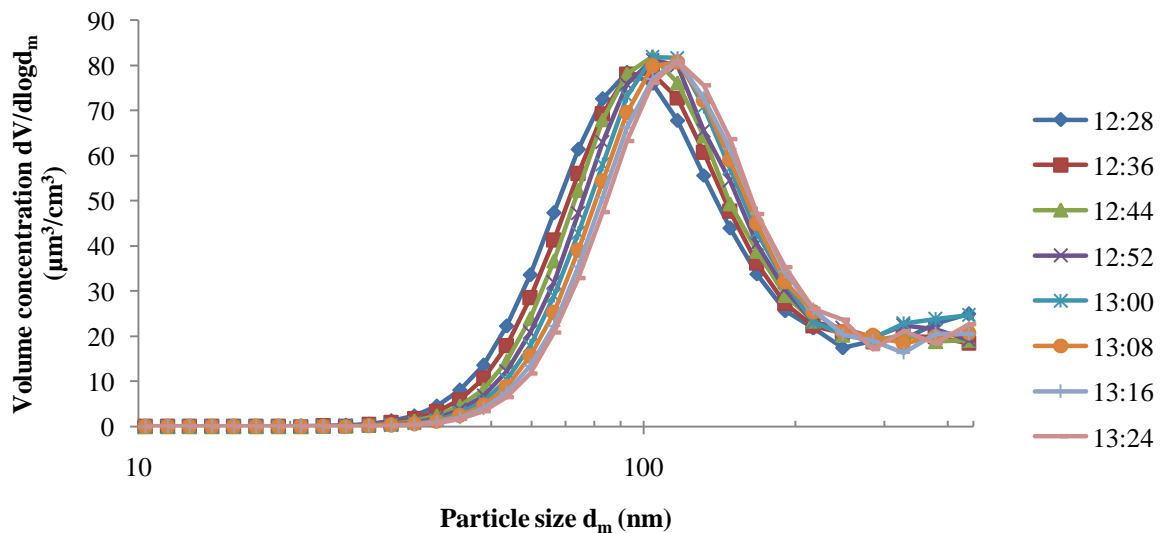


Figure 5.15: Volume distribution of the second experiment with the Peugeot 405.

The AMS results from the second experiment (Figure 5.16) showed the same results as the first experiment i.e. no drastic change in organic mass over time. Figure 5.17 and Figure 5.18 shows the result from the elemental analysis; cf. Appendix A.2 for assumptions made in APES. The elemental analysis was restricted to organic compounds, thus nitrates were not included. One was performed in the beginning before the ozone was added and one in the end of the experiment after the ozone was injected. The analysis shows virtually no difference in composition of the particles. The oxygen has increased from 14 % to 15 % but that increase is too small to be able to draw any conclusions from.

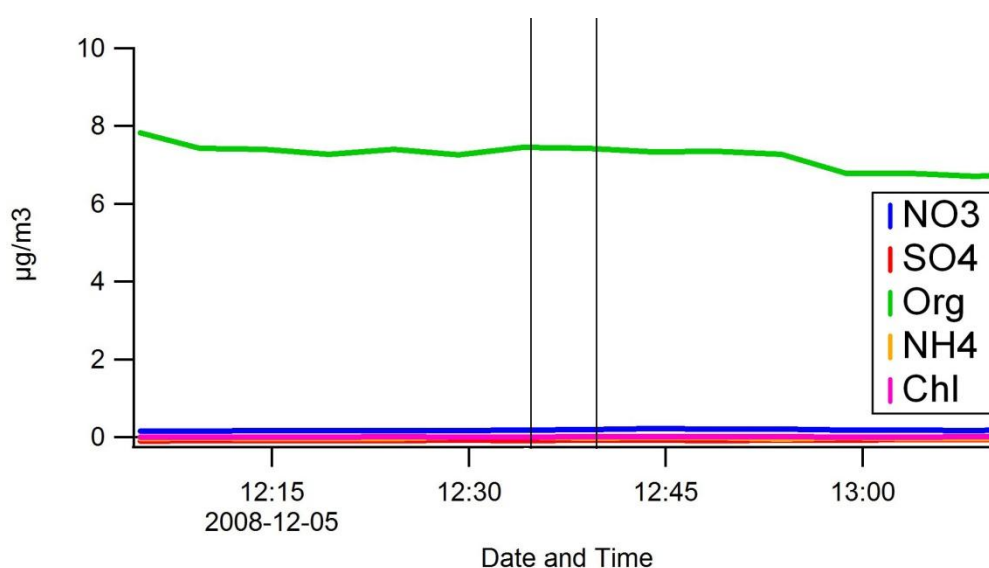


Figure 5.16: AMS, Mass vs. time of the second experiment with the Peugeot 405. The vertical lines indicate the time for ozone injection

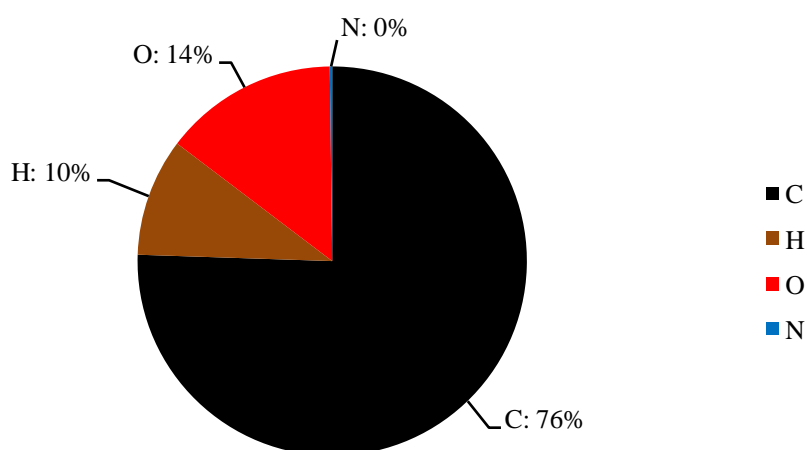


Figure 5.17: AMS, elemental analysis in the beginning of the second Peugeot 405 experiment just before the ozone was injected.

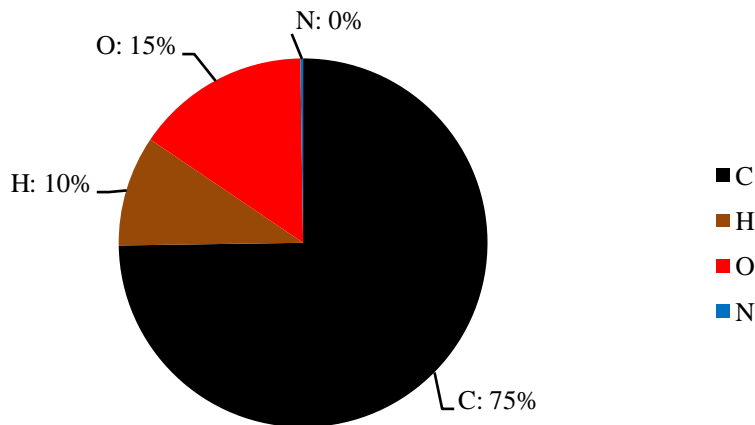


Figure 5.18: AMS, elemental analysis in the end of the second Peugeot 405 experiment 30-45 minutes after the ozone was injected.

The elemental analysis verifies that no oxidation process affecting the particle composition has occurred when the ozone was injected. Since the steel chamber was not ventilated before the ozone addition the concentration of particles was very high and also the NO_x level. The high amount of NO likely consumed all the ozone, which prevented any oxidation of the VOCs and diesel particles. In the ensuing experiments the chamber was ventilated to lower the concentration before the ozone was added.

5.5.2 Diesel car without particle trap - VW Passat

In this first experiment with the VW Passat the ozone was added at 15:01 during nine minutes up to a level of 400 ppb. Figure 5.19 and Figure 5.20 shows a large nucleation mode just after the ozone was added.

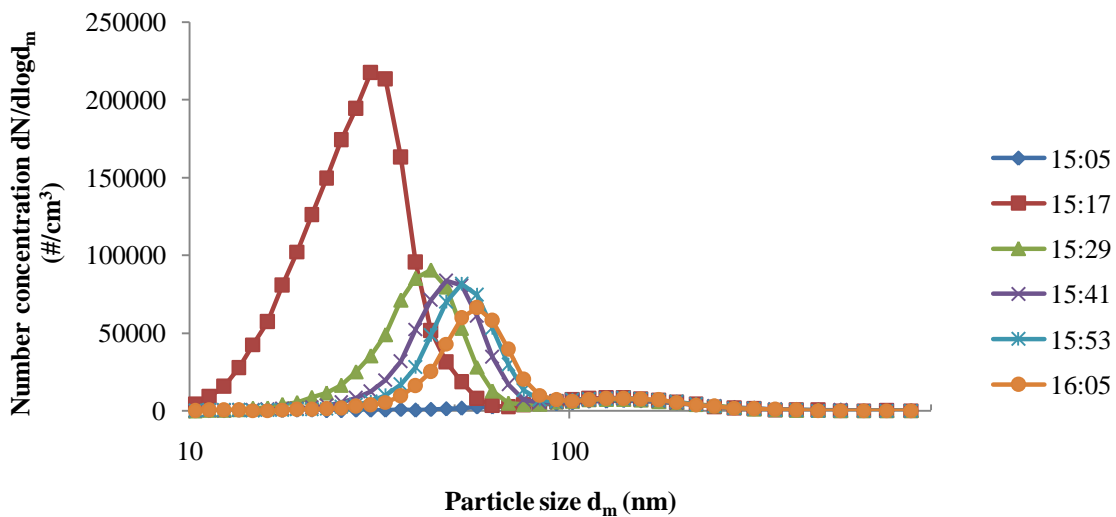


Figure 5.19: Number distribution of the first experiment with the VW Passat.

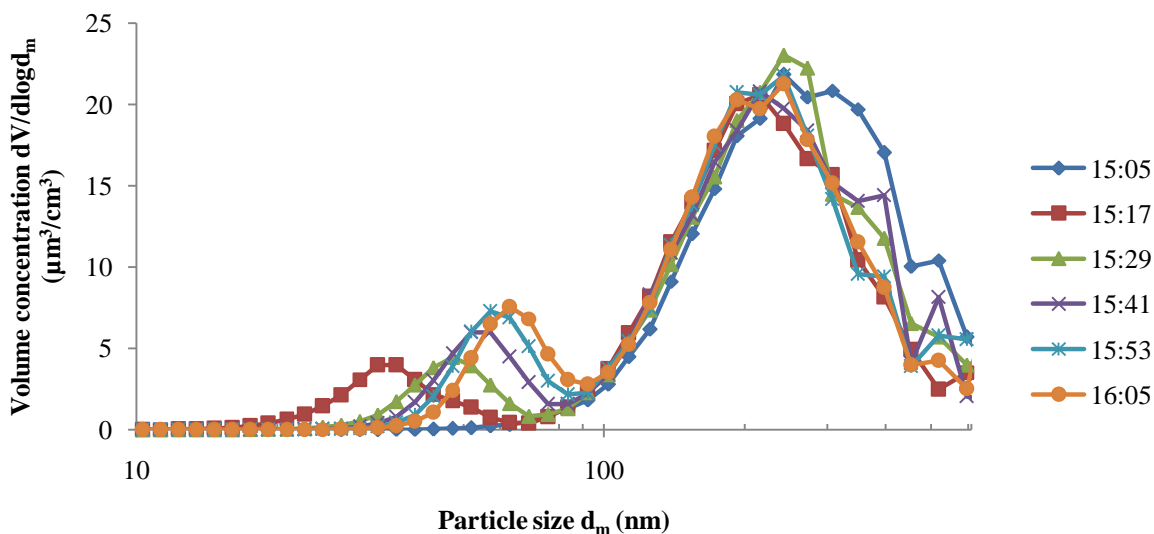


Figure 5.20: Volume distribution of the first experiment with the VW Passat.

In Figure 5.21 the organic and NO_3 mass increased drastically after the ozone was added. Figure 5.22 and Figure 5.23 shows the mass distribution from the AMS in the beginning before ozone and in the end after ozone was injected. There is a large difference in the mass distribution; the peak is moved from about 80 nm to 180 nm. The volume concentration of the SMPS (Figure 5.20) is stable at about 215 nm. In Figure 5.24 and Figure 5.25 the SMPS data has been manually fitted to the AMS data to assess the effective density, cf. Appendix A.1.

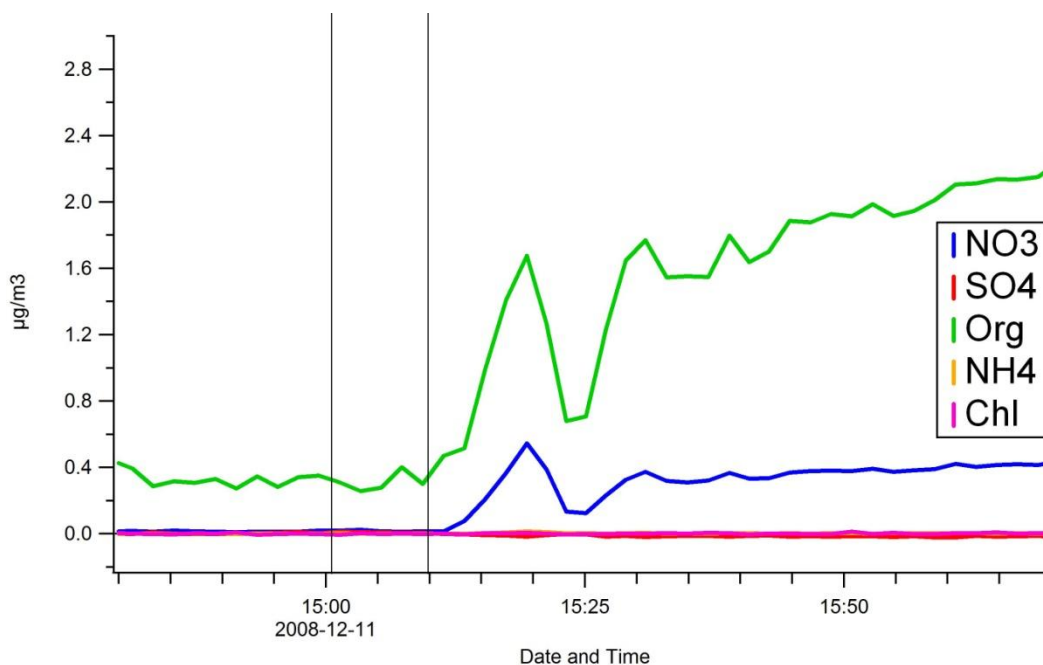


Figure 5.21: AMS, mass vs. time of the first experiment with the VW Passat. The vertical lines indicate the time for ozone injection

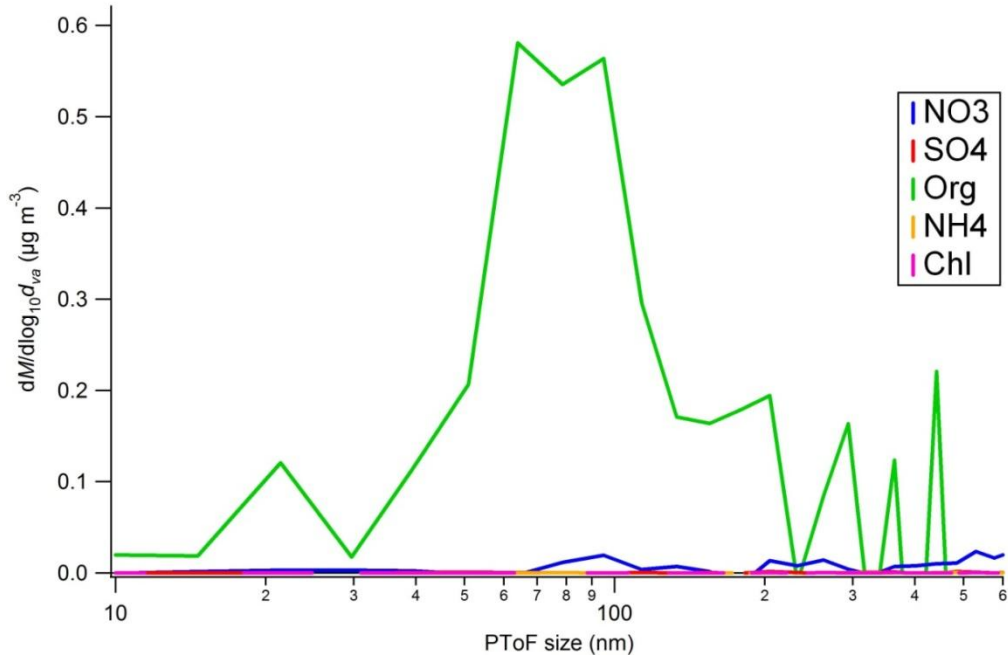


Figure 5.22: AMS, mass distribution in the beginning of the first VW Passat experiment just before ozone was injected.

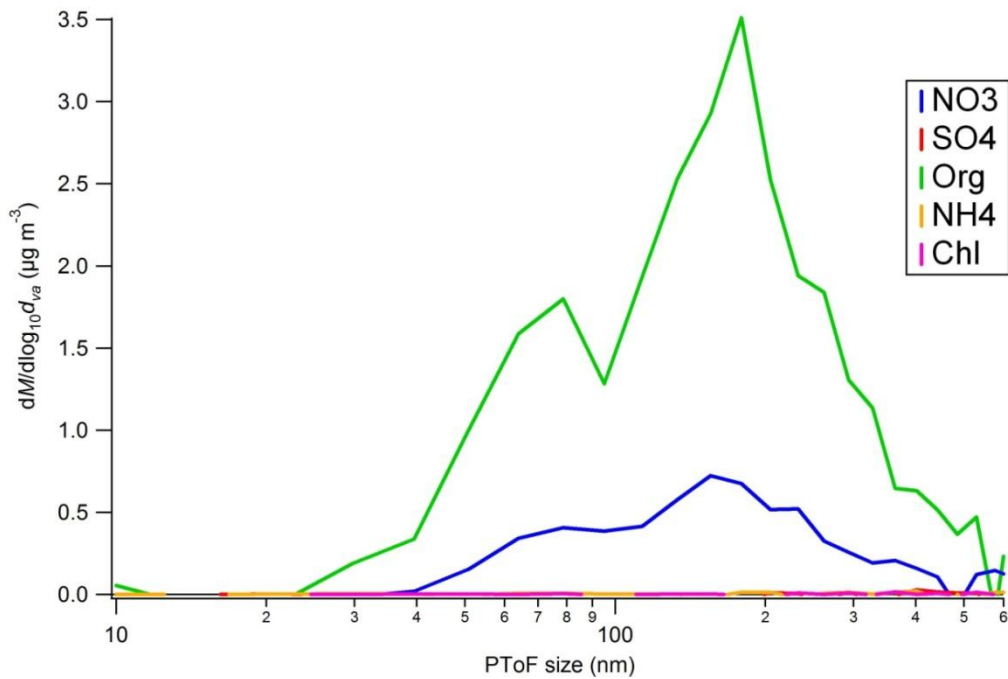


Figure 5.23: AMS, mass distribution in the end of the first VW Passat experiment 60 minutes after ozone was injected.

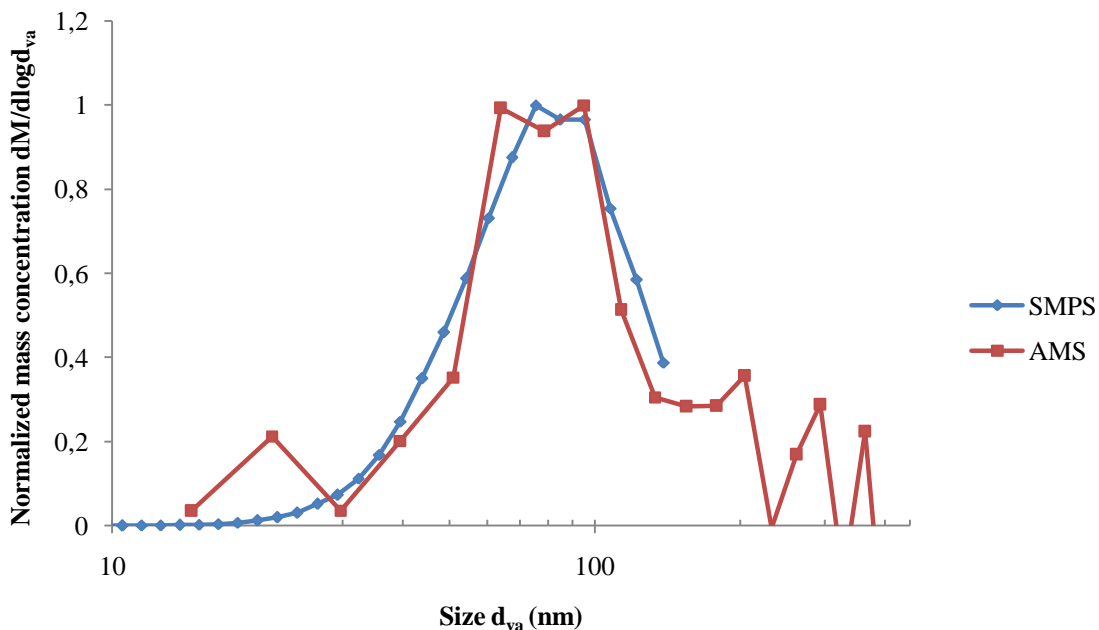


Figure 5.24: Normalized mass size distribution from the AMS and the SMPS. The SMPS distribution was shifted to vacuum aerodynamic diameter using the fitted effective density ($0,35 \text{ g/cm}^3$). Beginning of the first VW Passat experiment just before ozone was injected.

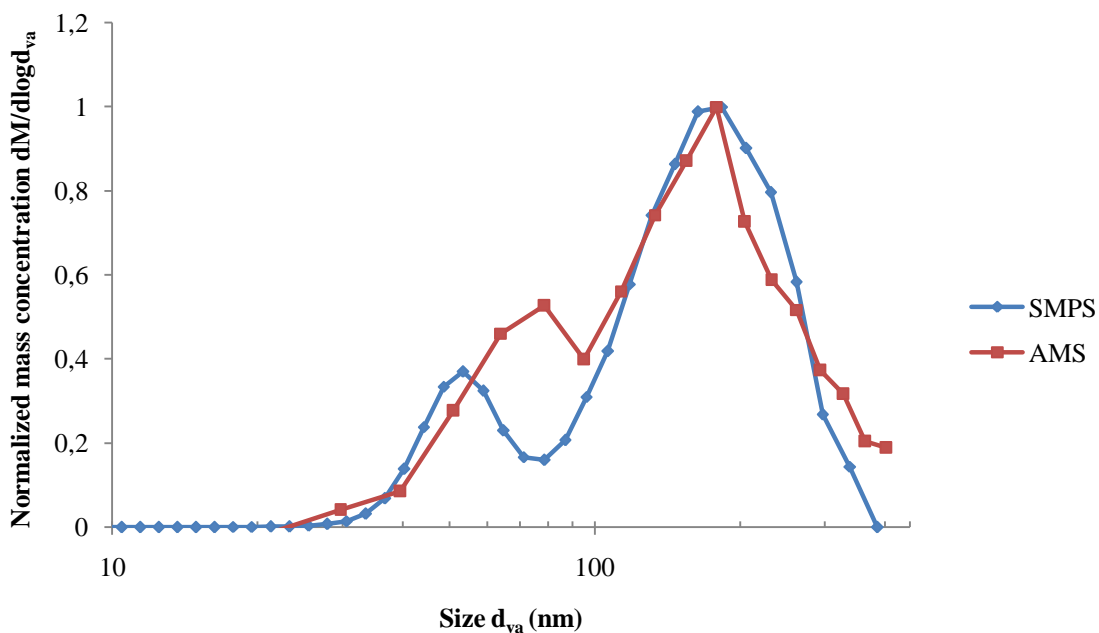


Figure 5.25: Normalized mass size distribution from the AMS and the SMPS. The effective density was fitted to $0,85 \text{ g/cm}^3$. End of the first VW Passat experiment 60 minutes after ozone was injected.

A leather armchair was left by mistake in the steel chamber during the experiment. The nucleation mode probably originates from the reaction between ozone and VOC emissions from

the leather armchair. The fluctuation in the mass increase in the AMS (Figure 5.21) could be an effect of spatially uneven ozone concentration.

The AMS showed large difference in mass distribution (Figure 5.22 and Figure 5.23) while the SMPS was stable (Figure 5.20), this implies that the mass of the particles had increased while their mobility diameter was equal. Figure 5.24 and Figure 5.25 shows an increase in effective density from 0,35 to 0,85 g/cm³. The same fitting was also made for the small nucleation mode (left peak in Figure 5.25) and the result showed an effective density of 1,25 g/cm³. Experiments made by Bahreini et al. 2005 showed that the effective density for secondary organic aerosols formed by nucleation processes was $1,39 \pm 0,05$ g/cm³ which agrees with our result. The increase in effective density from 0,35 to 0,85 g/cm³ means that the agglomerated particles have grown about 2,5 times in vacuum aerodynamic diameter after the ozone injection. Because the mass increases linearly with the effective density for a constant mobility diameter, there is also a corresponding increase in mass of the soot agglomerates. This is due to condensation of oxidized VOCs on the agglomerates. When VOCs condenses on agglomerates the cavities will be filled with VOCs. Since the boundary size is unchanged, the mobility diameter will not be affected. But the mass of the agglomerate will increase (Figure 5.26). By determining the effective density before and after an oxidation process, the mass-rate of condensation can be determined. On the contrary, the (vacuum) aerodynamic diameter will increase as the effective density increases upon condensation. Since the aerodynamic diameter depends on both the mass and drag force.

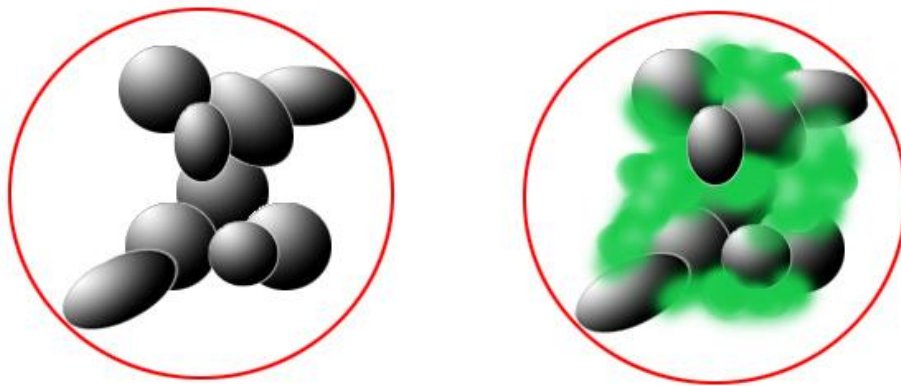


Figure 5.26: Fresh soot agglomerate (left) and condensed VOCs on soot agglomerate (right). The mobility diameter (circle) is the same but the mass is different.

The second measurement was similar to the first, but without any disturbing furniture in the steel chamber. The results showed (Figure 5.27 and Figure 5.28) that the SMPS system does not monitor any change in the diesel aerosol. The ozone was added during 9 minutes at 17:00.

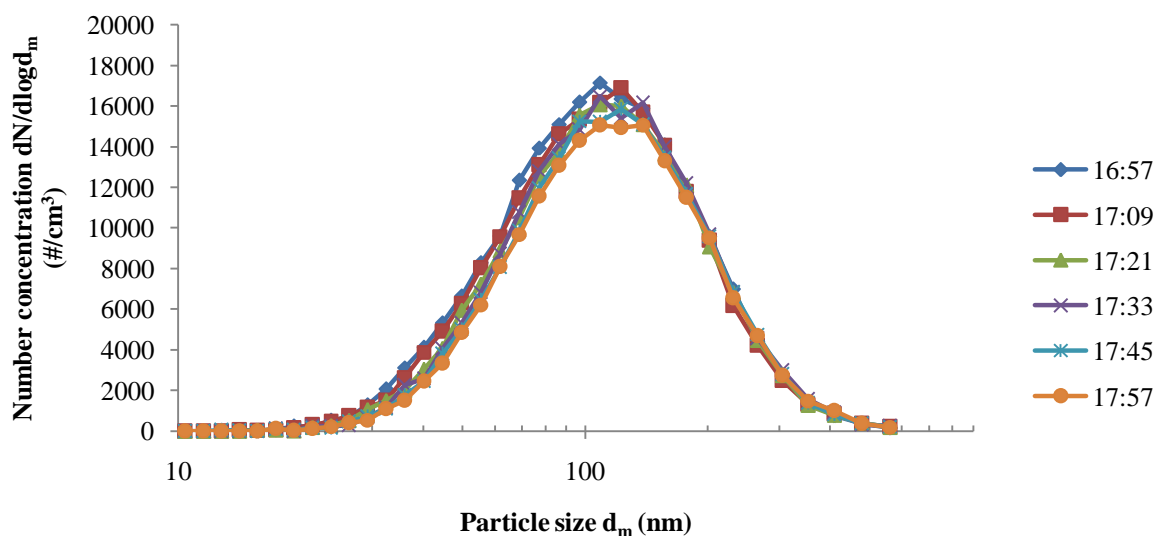


Figure 5.27: Number distribution of the second experiment with the VW Passat.

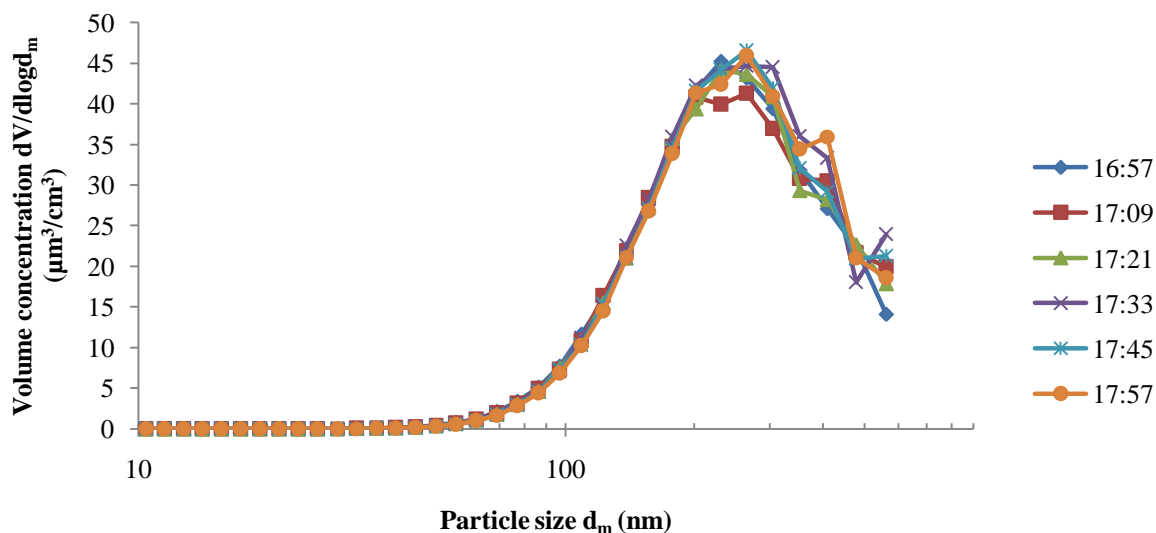


Figure 5.28: Volume distribution of the second experiment with the VW Passat.

Figure 5.29 shows a slight increase in organic and NO_3 mass after the ozone was injected. To investigate this further a high resolution analysis was performed (Figure 5.30). The figure shows how $\text{C}_2\text{H}_3\text{O}$ and C_3H_7 vary over time in m/z 43 (the most abundant organic fragment in the mass spectrum). The C_3H_7 peak is virtually unaffected by the addition of ozone, while the $\text{C}_2\text{H}_3\text{O}$ peak increases from close to zero to a high value upon ozone addition. In the

elementary analysis in Figure 5.31 and Figure 5.32 it is possible to see that the oxygen fraction has increased from 11% to 17% .

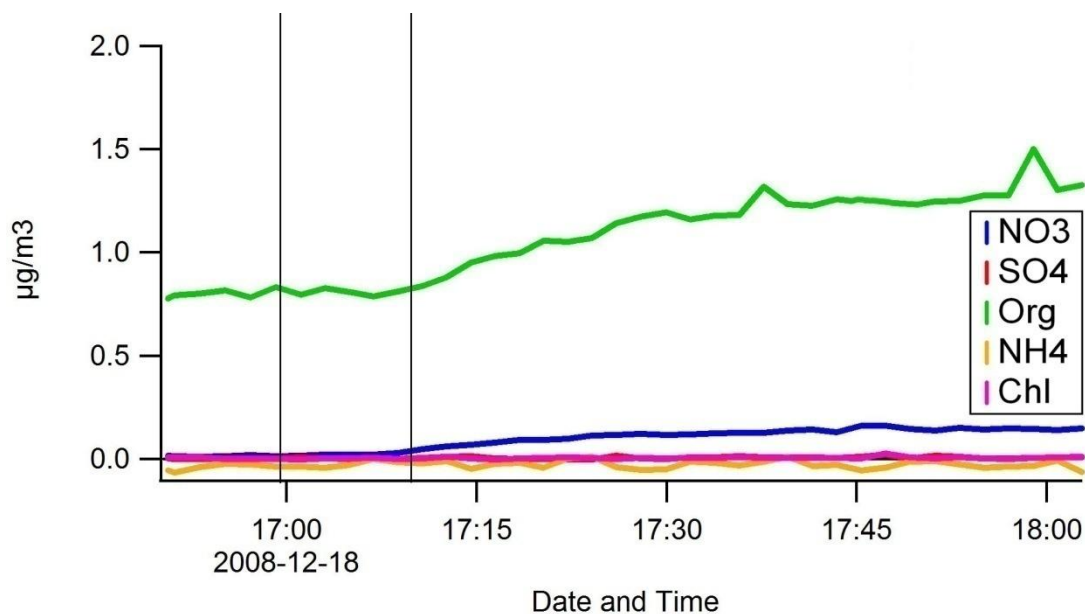


Figure 5.29: AMS, mass vs. time of the second experiment with the VW Passat. The vertical lines indicate the time for ozone injection

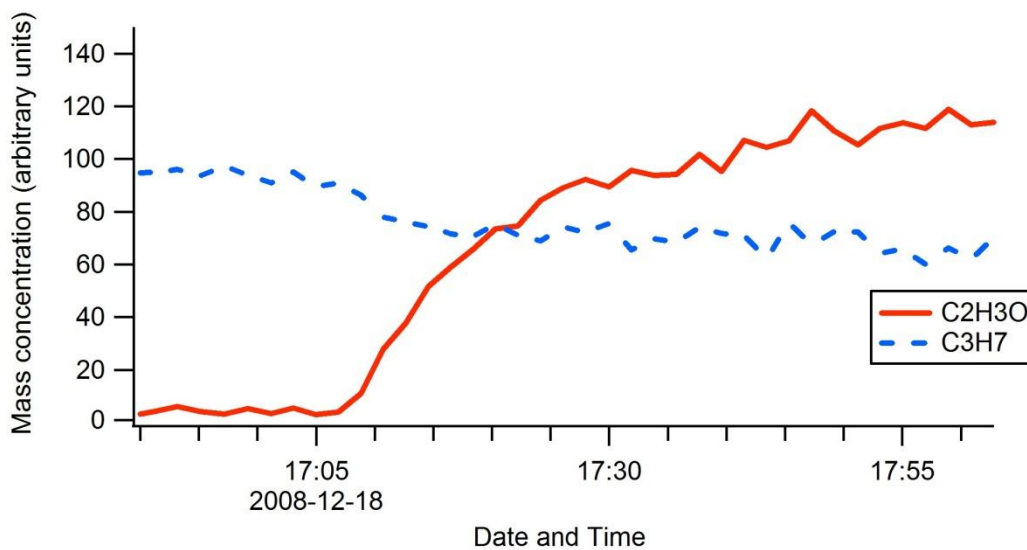


Figure 5.30: AMS, High resolution analysis of m/z 43 of the second experiment with the VW Passat.

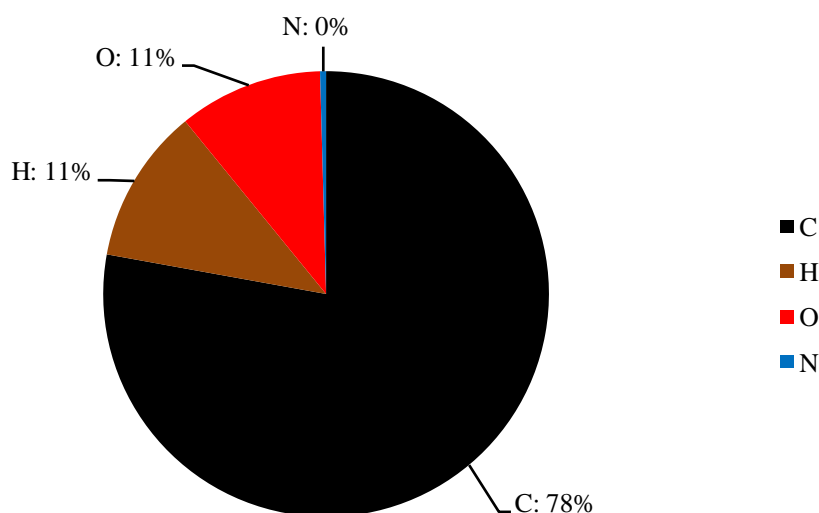


Figure 5.31: AMS, elemental analysis in the beginning of the second VW Passat experiment just before the ozone was injected.

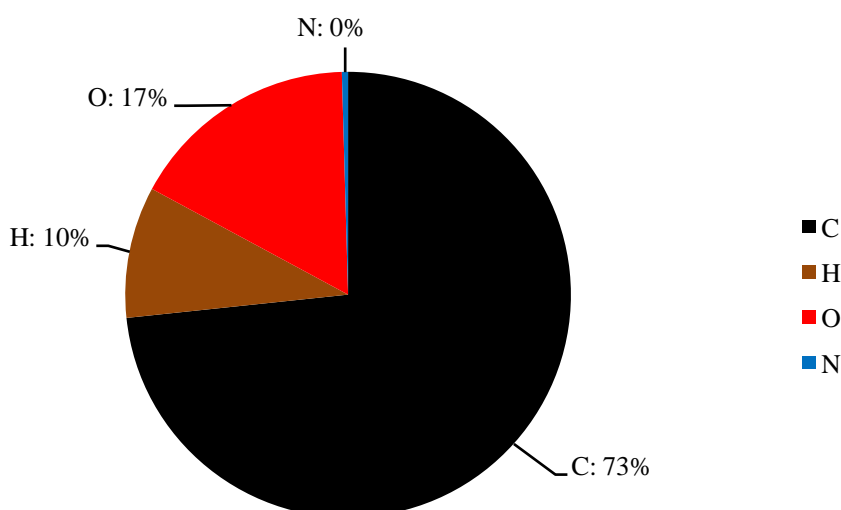


Figure 5.32: AMS, elemental analysis in the end of the second VW Passat experiment 30-45 minutes after the ozone was injected.

This experiment confirms that the nucleation mode in the previous experiment was due to the leather armchair in the steel chamber, since no nucleation mode appeared in this experiment. The SMPS showed no significant difference in volume concentration after the ozone was added. However the AMS showed signs of oxidation in the particles. Figure 5.29 shows an increase in organic mass after the ozone was added and this is also confirmed with the high resolution analysis (Figure 5.30). This shows that the fresh engine emissions mainly consist of non-oxidized hydrocarbons, while condensed secondary aerosol is oxidized. Thus the primary and secondary components are clearly different in composition.

The data concludes that VOCs had condensed on the agglomerates and that ozone contributes to changes in the diesel aerosol structure and composition. The furniture in the first experiment enhanced the oxidation process, but oxidation was also present in the second experiment.

5.5.3 Diesel car with particle trap - Peugeot 307 SW

This car was equipped with a particle trap which reduces the amount of particles in the exhaust air. The results in Figure 5.33 and Figure 5.34 show very small concentrations (number and volume), which implies that the particle trap worked. To achieve those low concentrations the car had to run for about 30 minutes. After the ozone was added during 9 minutes at 15:08, Figure 5.33 shows signs of a weak nucleation mode, while Figure 5.34 shows no significant change.

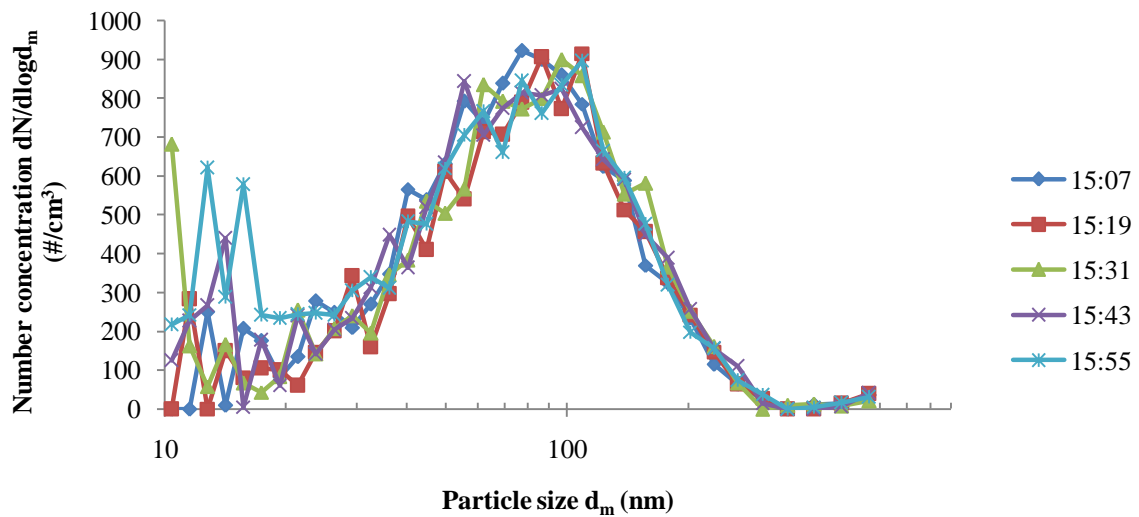


Figure 5.33: Number distribution of the experiment with the Peugeot 307 SW.

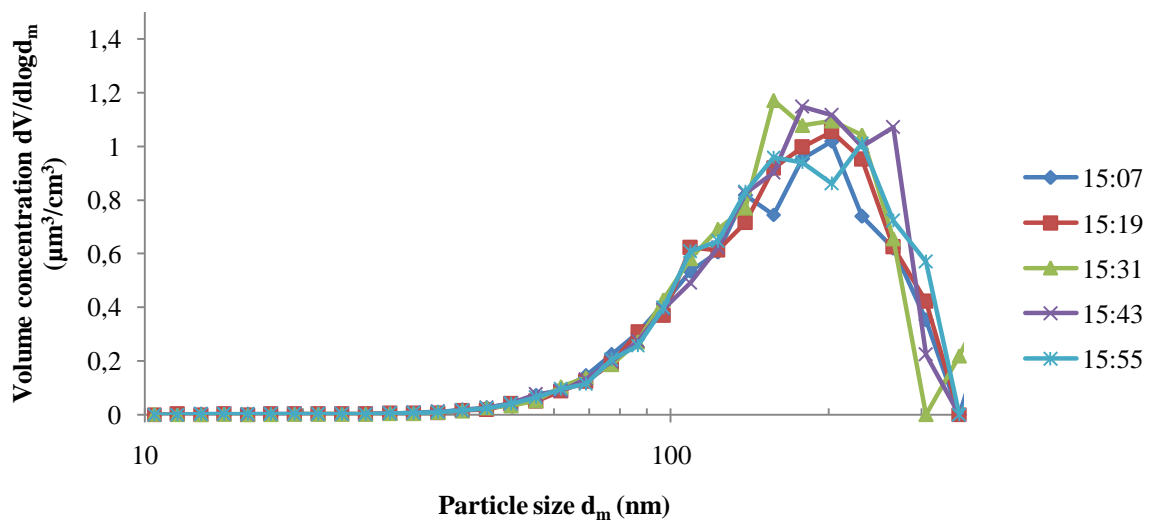


Figure 5.34: Volume distribution of the experiment with the Peugeot 307 SW.

The nucleation mode is probably due to the small number concentration. The lack of particles for the VOCs to condense on causes them to nucleate. Unfortunately the AMS was out of order during this measurement and therefore it is difficult to make any deeper analysis of the results. But the mass concentration was probably too low to get any quantitative results from the AMS.

6 Conclusions and future work

The main conclusion from the ageing experiments is that different cars have different exhaust aerosols and therefore the result also varies. The best suited cars for ageing experiment in our case is the VW Passat since it is a fairly new car and without any particle trap.

When using ozone in experiments it is important to dilute the exhaust so the NO level is lower than the injected ozone concentration. Otherwise the ozone will mainly react with the NO. Therefore a car with particle trap is not to prefer since dilution the exhaust will result in a particle concentration lower than desired.

Ozone will not cause nucleation in diesel exhausts, when measuring on ambient concentrations but it is responsible for condensation of VOCs on soot agglomerates. Condensation processes could only be detected by using a combination of SMPS and AMS. Therefore it is important to have a well functioning AMS in future experiments.

It is very important that the measurement chamber is clean and free from any foreign objects that can react with ozone.

The concept with the Teflon chamber mounted in the steel chamber seems to be promising, the cooling, ventilation and UV-lights work sufficiently. The Teflon chamber will though need more cleaning before it is ready to be used in future experiments. A few parts of the inlet/outlet air system could be changed to parts of better suited material to minimize contamination of the air. The used armatures could be replaced with a custom made armature. Equipment for monitoring the temperature and RH inside the Teflon chamber would be preferable in future experiments.

More experiments with a car with particle trap are needed. The main work that needs to be done in the future is experiments where diesel exhausts are exposed to UV-light to investigate the secondary aerosol formation caused by UV-light. It is possible that UV exposure leads to a stronger secondary aerosol formation as ozone only reacts selectively with a small group of compounds such as alkenes.

References

Aerodyne Research Inc. 2009, *AMS manual*. visited 2009-01-23, “<http://www.aerodyne.com/cacc/AMSUsersManualWebPages/aerodynemanual/newcalibrations.htm>”

Akselsson Roland, Bohgard Mats, Gudmundsson Anders, Hansson Hans-Christen, Martinsson Bengt and Svenningsson Birgitta, *Aerosoler*. Lunds Tekniska Högskola & NOSA, 1994

Bahreini R., Keywood M. D., Ng N. L., Varutbangkul V., Gao S., Flagan R.C., Seinfeld J. H., Worsnop D. R. and Jimenez J. L.. (2005). *Measurements of Secondary Organic Aerosol from Oxidation of Cycloalkenes, Terpenes, and m-Xylene Using an Aerodyne Aerosol Mass Spectrometer*. Environmental Science & Technology, 39, 5674-5688

Burtscher H.. (2005). *Physical characterization of particulate emissions from diesel engines: a review*. Aerosol Science, 36, 896-932

Canagaratna M.R., Jayne J.T., Jimenez J.L., Allan J.D., Alfarra M.R., Zhang Q., Onasch T.B., Drewnick F., Coe H., Middlebrook A., Delia A., Williams L.R., Trimborn A.M., Northway M.J., DeCarlo P.F., Kolb C.E., Davidovits P., and Worsnop D.R.. (2007). *Chemical and microphysical characterization of ambient aerosols with the aerodyne aerosol mass spectrometer*. Mass Spectrometry Reviews, 26, 185-222

Carter William P.L., Cocker David R., Fitz Dennis R., Malkina Irina L., Bumiller Kurt, Sauer Claudia G., Pisano John T., Bufalino Charles, Song Chen. (2005). *A new environmental chamber for evaluation of gas-phase chemical mechanisms and secondary aerosol formation*. Atmospheric Environment, 39, 7768-7788

DeCarlo Peter F., Kimmel Joel R., Trimborn Achim, Northway Megan J., Jayne John T., Aiken Allison C., Gonin Marc, Fuhrer Katrin, Horvath Thomas, Docherty Kenneth S., Worsnop Doug R., and Jimenez Jose L. (2006). *Field-Deployable, High-Resolution, Time-of-Flight Aerosol Mass Spectrometer*. Analytical Chemistry, 78, 8281-8289

DeCarlo Peter F., Slowik Jay G., Worsnop Douglas R., Davidovits Paul, and Jimenez Jose L.. (2004). *Particle Morphology and Density Characterization by Combined Mobility and Aerodynamic Diameter Measurements. Part 1: Theory*. Aerosol Sci. Technol., 38, 1185-1205

ECO Physics [A], *CLD 700 AL med: Addendum to the instruction manual CLD 700 AL*. 1996

ECO Physics [B], *CLD 700 AL*, visited 2009-01-30, “http://www.ecophysics.com/data/leaflets/7000al_e.pdf”

Forsberg Bertil, Hansson Hans-Christen, Johansson Christer, Areskoug Hans, Persson Karin and Järvholm Bengt. (2005). *Comparative Health Impact Assessment of Local and Regional Particulate Air Pollutants in Scandinavia*. Royal Swedish Academy of Sciences, Vol.34, No.1, February 2005, 11-19

Hallquist M., Wenger J. C., Baltensperger U., Rudich Y., Simpson D., Claeys M., Dommen J., Donahue N. M., George C., Goldstein A. H., Hamilton J. F., Herrmann H., Hoffmann T., Iinuma Y., Jang M., Jenkin M., Jimenez J. L., Kiendler-Scharr A., Maenhaut W., McFiggans G., Mentel Th. F., Monod A., Prévôt A. S. H., Seinfeld J. H., Surratt J. D., Szmigielski R., and Wildt J.. (2009). *The formation, properties and impact of secondary organic aerosol: current and emerging issues*. Atmos. Chem. Phys. Discuss., 9, 3555-3762

Hinds William C., *Aerosol Technology, properties, behavior and measurement of airborne particles*. Second edition. John Wiley and Sons, Inc., New York, 1999

Isaxon Christina, *Controlled human exposures to aerosol particles – Design, characterization and evaluation of aerosol generation system and chamber exposures*. Master Thesis, Ergonomics and Aerosol technology, Lund University, 2008

JACO, *Compression tube fittings product catalog & price list*. 2007

Jacob Daniel J., *Introduction to atmospheric chemistry*. Princeton University Press, Princeton, 1999

Jayne John T., Leard Danna C., Zhang Xuefeng, Davidovits Paul, Smith Kenneth A., Kolb Charles E., and Worsnop Douglas R. (2000). *Development of an Aerosol Mass Spectrometer for Size and Composition Analysis of Submicron Particles*. Aerosol Science and Technology, 33, 49-70

Maricq M. Matti. (2007). *Chemical characterization of particulate emissions from diesel engines: A review*. Aerosol Science, 38, 1079-1118

Nilsson Patrik, *Design and Characterization of a Diesel-aerosol Generating System*. Master Thesis, Ergonomics and Aerosol Technology, Lund University 2009

NILU, *EMEP manual for sampling and chemical analysis*. November 2001

Pagels Joakim, *Aerosol formation from anthropogenic combustion sources*. Formas Application abstract, Lund, 2007

Pathak Ravikant, Donahue Neil M. and Pandis Spyros N.. (2008). *Ozonolysis of β -Pinene: Temperature Dependence of Secondary Organic Aerosol Mass Fraction*. Environmental Science & Technology, 42, 5081-5086

Paulsen Dwane, Dommen Josef, Kalberer Markus, Prvt Andr S.H., Richter Ren, Sax Mirjam, Steinbacher Martin, Weingartner Ernest and Baltensperger Urs. (2005). *Secondary Organic Aerosol Formation by Irradiation of 1,3,5-Trimethylbenzene-NO-HO in a New Reaction Chamber for Atmospheric Chemistry and Physics*. Environmental Science & Technology, 39, 2668-2678

Philips, *CLEO Performance 100W –R SLV Product family description*. 2009

Robinson Allen L., Donahue Neil M., Shrivastava Manish K., Weitkamp Emily A., Sage Amy M., Grieshop Andrew P., Lane Timothy E., Pierce Jeffrey R., Pandis Spyros N.. (2007). *Rethinking Organic Aerosols: Semivolatile Emissions and Photochemical Aging*. Science, 315, 1259-1262

Sehlstedt Maria, Forsberg Bertil, Westerholm Roger, Boman Christoffer, Sandström Thomas. (2007). *The Role of Particle Size and Chemical Composition for Health Risks of Exposure to Traffic Related Aerosols – A Review of the Current Literature*. Available on 2009-02-11 at <http://www.pff.nu/upload/EMFO/resultat/Partiklar/EMFO%20litteraturstudie%20-Trafikrelaterade%20partiklar%20och%20h%C3%A4lsoeffekter%20-%20Final%20report%20071212.pdf>

Seinfeld John H., Pandis Spyros N., *Atmospheric chemistry and physics, From Air Pollution to Climate Change*. Second Edition. John Wiley and Sons Inc, Hoboken, New Jersey, 2006

Thermo Electronics, *TEOM[®] Series 1400a Ambient Particulate Monitor*. East Greenbush NY USA

TSI [A], *Model 3934 SMPS Instruction Manual, Appendix B Theory of operation*.

TSI [B], *Model 3010 Condensation Particle Counter, Product information*

Acknowledgements

We would like to thank everyone who helped us during this Master thesis.

Especially thanks to our supervisor Dr. Joakim Pagels for excellent guidance, encouragement and for always have taken time for discussions and questions.

Dr. Anders Gudmundsson for advices and for handing us a very nice office.

The excellent collaboration with fellow Master thesis workers Axel Eriksson and Patrik Nilsson has been very valuable for our project.

Professor Erik Swietlicki for discussions and questions.

Lennart Strömberg for helping us with mechanical matters.

Robert Olsson for computer support.

Karin Öhrvik for administrative issues.

Dr. Adam Kristensson for the study trip to university of Copenhagen.

We also thank Andreas Dahl, Pontus Rohldin, Erik Nilsson, Dr. Jakob Löndahl, Christina Isaxon and Dr. Aneta Wierzbicka for answering whatever questions we had.

Appendix A

A.1 (Manual fitting of effective density)

The effective density is determined by matching normalized distribution peaks from the AMS (mass distribution) and the SMPS (volume distribution). The particle size from the SMPS is converted to vacuum aerodynamic size by multiplication with the effective density and plotted against the AMS data. The effective density is manually varied until the curves fit against each other.

A.2 (Assumptions made in APES)

Figure A.1 shows the standard assumptions made in APES when calculating the elemental composition. We used all the default settings, except removing CH_2N from the analysis. The fitted curve to CH_2N is a small fraction on the edge of the N_2 peak (Figure A.2). The major contribution to m/z 28 comes from N_2 , which is the dominating molecule in the ambient air; therefore m/z 28 is dominating in the mass spectrum. The analyze software (SQUIRREL, PIKA and APES) does not include the contribution from ambient air molecules and therefore N_2 is removed but CH_2N is not. Since m/z 28 is such a dominating peak CH_2N will be overrepresented in the APES analysis.

The screenshot shows the 'Analytical Procedure (for OM) Elemental Separation (APES) 1.0' window. The interface includes a menu bar (File, Edit, Data, Analysis, Macros, Windows, Panel, Misc, Help, AMS) and a title bar ('DieselOzone18DecHIGHRES - Igor Pro 6.04 - [EA_panel]'). The main content area is divided into several steps:

- Step 0:** Create atomic mass fraction of selected HR fragments. (Optional) View table of atomic mass fractions. Set to default.
- Step 1:** Select options for elemental analysis. Set to default.
 - Step 1A: Convert nans to 0? Step 1B: Choose the todo wave: slutet
 - Step 1C: Choose how much CO_2^+ in OM is calculated.
 - Estimate CO_2^+ as CO_2 HR stick less gas $\text{CO}_2 = 370.0$ ppm.
 - Estimate CO_2^+ as CO_2 HR stick less gas CO_2 (ppm) in wave: []
 - Sensitivity (multiplicative) factor for estimated gas $\text{CO}_2 = 1.00$
 - Step 1D: Choose how much CO^+ in OM is calculated.
 - Estimate CO^+ as 1.000 times the elemental analysis stick of CO_2
 - Estimate CO^+ as 100% of measured CO^+ Pika HR stick.
 - Step 1E: Choose how much H_2O^+ , OH^+ , O^+ in OM are calculated.
 - Estimate H_2O^+ as 0.225 times the elemental analysis stick of CO_2
 - Estimate OH^+ as 0.250 times the elemental analysis stick of H_2O
 - Estimate O^+ as 0.040 times the elemental analysis stick of H_2O
 - Estimate each as 1.000 times the H_2O , OH , O HR Pika sticks.
- Check values in steps 1C, 1D, 1E for consistency with frag_organic entries in Squirrel.
- Step 1F: Choose whether to include inorganic ion fragment families in OM.
 - OH family that is not H_2O , OH and O
 - SO family
 - NH family
 - NO family
- Step 1G: Choose individual inorganic ion fragments to include/exclude.
 - List of additional non-C HR fragments to include in OM: []
 - List of HR fragments to exclude in OM: (i.e. " $\text{H}_2\text{O}_2, \text{H}_3\text{O}^+$ ") CH₂N
- Step 1H: Choose calibration factors.
 - H/C 0.910
 - O/C 0.750
 - N/C 0.960
 - S/C* 1.000
 - * This S/C value has not yet been measured or published. Use with caution!

Step 2: Calculate elemental ratios of HR sticks. New Plot?
OR
Step 2: Calculate average mass spectra of elemental values. New Plot?

- m/z in HR Space
- display using separate axes
- m/z summed to UMR
- display as stacked bars

Figure A.1: Elemental analysis software APES

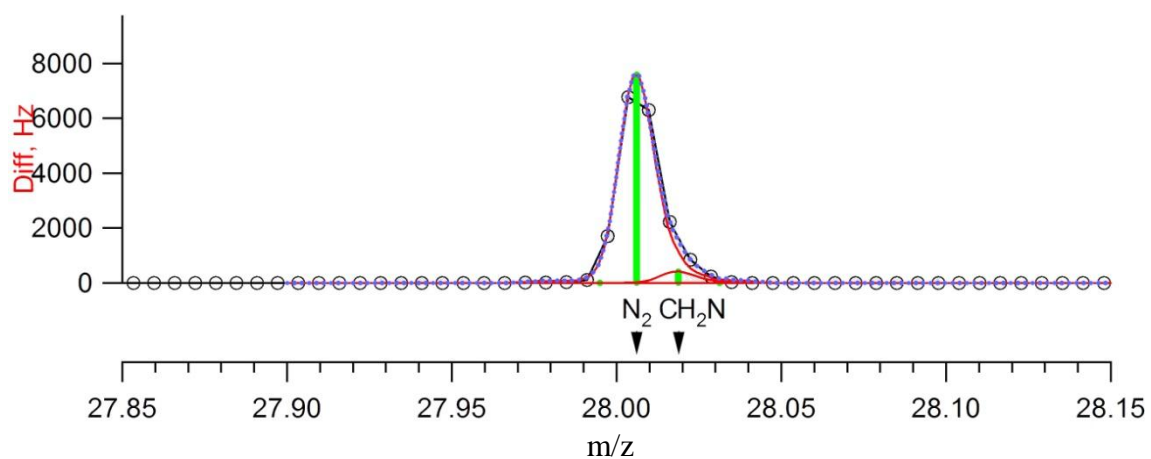


Figure A.2: m/z 28 from the high resolution software PIKA showing the N_2 and CH_2N peak.

Appendix B

B.1 (Checklist for diesel/ozone experiments in simulation chamber)

Checklist

Date:

- ◆ Check the flow on the SMPS, conduct a zero test (turn of the voltage supply to confirm that the CPC measures zero particles).
- ◆ Check the flow rate in the air supply to the ozone generator.
- ◆ Double check that the chamber is empty and start the domestic fan in the chamber (voltage 130-140 V).
- ◆ Ventilate the chamber until desired concentration is reached after the car has been turned off.
- ◆ Close the inlet/outlet to the chamber, climate control and exhaust fan.
- ◆ Start the ozone generation, maximum effect (4,5 min = 200 ppb, 9 min = 400 ppb).
- ◆ End the experiment after desired time.
- ◆ Do not forget to open inlet/outlet to the chamber and start the climate control and exhaust fan.

Times:

Car start	
Car stop	
Closing of the inlet/outlet	
Start of ozone generation	
End	



LUND UNIVERSITY